

Tight-binding theory of spin-spin interactions, Curie temperatures, and quantum Hall effects in topological (Hg,Cr)Te in comparison to non-topological (Zn,Cr)Te, and (Ga,Mn)N

Cezary Śliwa^{1,2,*} and Tomasz Dietl¹

¹*International Research Centre MagTop, Institute of Physics,
Polish Academy of Sciences, al. Lotników 32/46, PL-02668 Warsaw, Poland*

²*Institute of Physics, Polish Academy of Sciences, al. Lotników 32/46, PL-02668 Warsaw, Poland*
(Dated: 2024-06-05)

Earlier theoretical results on p - d and d - d exchange interactions for zinc-blende semiconductors with Cr^{2+} and Mn^{3+} ions are revisited and extended by including contributions beyond the dominating ferromagnetic (FM) superexchange term [i.e., the interband Bloembergen-Rowland-Van Vleck contribution and antiferromagnetic (AFM) two-electron term], and applied to topological Cr-doped HgTe and non-topological (Zn,Cr)Te and (Ga,Mn)N in zinc-blende and wurtzite crystallographic structures. From the obtained values of the d - d exchange integrals J_{ij} , and by combining the Monte-Carlo simulations with the percolation theory for randomly distributed magnetic ions, we determine magnitudes of Curie temperatures $T_C(x)$ for $\text{Zn}_{1-x}\text{Cr}_x\text{Te}$ and $\text{Ga}_{1-x}\text{Mn}_x\text{N}$ and compare to available experimental data. Furthermore, we find that competition between FM and AFM d - d interactions can lead to a spin-glass phase in the case of $\text{Hg}_{1-x}\text{Cr}_x\text{Te}$. This competition, along with a relatively large magnitude of the AF p - d exchange energy $N_0\beta$ can stabilize the quantum spin Hall effect, but may require the application of tilted magnetic field to observe the quantum anomalous Hall effect in HgTe quantum wells doped with Cr, as confirmed by the Chern number determination.

I. INTRODUCTION

Extensive studies of (Ga,Mn)As and other dilute ferromagnetic semiconductors (DFSs), in which band holes mediate exchange interactions and magnetic anisotropies, have allowed demonstrating several functionalities, such as the effects of light, electric fields and currents on the magnetization magnitude and direction [1, 2]. Similarly striking phenomena have been discovered in DFSs without band carriers, the prominent examples being the piezo-electro-magnetic effect in wurtzite (Ga,Mn)N [3] or the parity anomaly [4] and the quantum anomalous Hall effect [5, 6] in topological (Bi,Sb,Cr)Te and related systems [7–10], the latter opening a prospect for developing a functional low magnetic field resistance standard [11–14]. In agreement with indications coming from synchrotron studies of magnetic configurations of V and Cr impurities in (Bi,Sb)₂Te₃ [15], a theory developed by us for dilute magnetic semiconductors (DMS) such as topological (Hg,Mn)Te and topologically trivial (Cd,Mn)Te [16] shows that, if a spurious self-interaction term is disregarded, the Anderson-Goodenough-Kanamori superexchange dominates over the interband Bloembergen-Rowland-Van Vleck mechanism [5, 7–10] on the both sides of the topological phase transition in insulator magnetic systems [16]. Ferromagnetic insulators also serve to generate giant Zeeman splitting of bands in adjacent layers: the quantum anomalous Hall effect in (Bi,Sb)Te/(Zn,Cr)Te quantum wells (QWs) [17] and topological superconductivity in InAs nanowires proximitized by an EuS layer [18] constitute just two re-

cent examples.

Exchange interactions between the spins of electrons residing in partially occupied d -shells, mediated by hybridization \tilde{V}_{hyb} between d shells of magnetic ions and p orbitals of neighboring anions, can be either ferromagnetic (FM) or antiferromagnetic (AFM), orbital dependent, and sensitive to Jahn-Teller distortions [19]. The progress in understanding the underlying mechanism of these interactions allowed to formulate Anderson-Goodenough-Kanamori rules [19], which predict the character of the interactions in a given system provided that the nature of the relevant chemical bonds is known. More recently, Blinowski, Kacman, and Majewski [20] — by a complex calculation involving the fourth-order perturbation theory in \tilde{V}_{hyb} — found that in tetrahedrally coordinated II-VI Cr-based dilute magnetic semiconductors the superexchange component of the spin pair interaction is FM. This FM coupling results from the partial filling of t_2 orbitals occurring for the high spin d^4 electronic configuration of the magnetic shell in the case of the substitutional Cr^{2+} ions in the tetrahedral environment. On the experimental side, FM ordering was indeed found in (Zn,Cr)Te but a meaningful determination of Curie temperature T_C as a function of the Cr concentration x is hampered by aggregation of Cr cations [21]. Accordingly, the values of $T_C(x)$ determined recently for high quality $\text{Zn}_{1-x}\text{Cr}_x\text{Te}$ epilayers [17] provide an upper limit of T_C expected for a random distribution of magnetic ions. The generality of the superexchange scenario was then demonstrated in the case of wurtzite (wz) (Ga,Mn)N containing randomly distributed Mn^{3+} ions, for which the experimental dependence $T_C(x)$ [22–24] was reasonably well explained theoretically employing Blinowski's *et al.* theory for the zinc-blende structure. Monte-Carlo simulations served to obtain $T_C(x)$ magni-

* sliwa@magtop.ifpan.edu.pl

tudes from the computed values of the exchange integrals J_{ij} for Mn spin pairs at the distances R_{ij} up to the 16th coordination sphere [23–25].

Here, the above-mentioned theoretical results for the d^4 configuration in DMS without band carriers are revisited and extended by including additional contributions beyond the superexchange, which results from the fourth order perturbation theory in \hat{V}_{hyb} , such as the interband Bloembergen-Rowland term [16, 26–31], known in the topological literature as the Van Vleck mechanism [5, 7–10]. Furthermore, our theory is developed for both zinc-blende and wurtzite semiconductors, allowing us to assess the crystal structure’s role in magnetic interactions. We also demonstrate quantitative agreement in the values of T_C obtained by the Monte-Carlo simulations and from the percolation theory for random ferromagnets [32]. This agreement makes us possible to determine $T_C(x)$ from $J(R_{ij})$ values for the whole x range, $0 < x < 1$, without Monte-Carlo simulations that are computationally expensive for disordered magnetic systems. The present developments are possible by making use of contemporary software tools for formula derivations, which allowed us to correct several inaccuracies in the original formulae [20] for superexchange between pairs of spins residing on d^4 shells. We also correct some previous inconsistencies in values of Mn parameters [25] and discuss our results in comparison to experimental data on $T_C(x)$ for wz-Ga $_{1-x}$ Mn $_x$ N [22–24] and zb-(Zn,Cr)Te [17].

Comparing the present results for Cr $^{2+}$ and Mn $^{3+}$ to the previously investigated Mn $^{2+}$ case [realized in (Hg,Mn)Te and (Cd,Mn)Te] [16], the superexchange term (denoted as hh) has the opposite sign for those two configurations. In contrast, the interband he and ee contributions behave similarly, i.e., he is FM at small distances between magnetic ions and AFM for distant pairs. Our results demonstrate, in agreement with experimental observations, that FM interactions prevail in the case of (Zn,Cr)Te and wz-(Ga,Mn)N. At the same time, our T_C values are much smaller compared to *ab initio* results [33], as local functional approximations tend to underestimate localized character of $3d$ orbitals in semiconductors.

According to our theory, the ferromagnetic hh term entirely dominates in (Ga,Mn)N. We show that the theoretical $T_C(x)$ magnitudes for wz-(Ga,Mn)Te are only slightly larger than experimental values, which may point out to an influence of the Jahn-Teller distortion neglected in the present approach.

However, the situation is more involved in the case of (Hg,Cr)Te and (Zn,Cr)Te. In those systems, due to the importance of the competition between FM and AFM couplings, the theoretically expected critical temperatures are rather sensitive to the employed tight-binding model of the host band structure. Actually, in the case of topological (Hg,Cr)Te, although the sign of Curie-Weiss temperatures points to a prevailing role of the FM interactions, a competition between FM and AFM contributions may result in the spin-glass freezing at low temper-

atures.

The striking properties of semiconductors with magnetic ions mentioned above result from strong $sp-d$ exchange interactions between effective mass carriers and electrons residing in open d shells of magnetic ions [34]. While the signs and magnitudes of $s-d$ and $p-d$ exchange integrals have been extensively studied theoretically [30, 35] and experimentally [36, 37] for wide band gap Cr-doped II-VI compounds and wz-(Ga,Mn)N, we present here theory of $sp-d$ coupling for Cr-doped topological HgTe. We show that the presence of Cr ions should improve the quantization accuracy of the quantum spin Hall effect in the paramagnetic phase. We also enquire on whether the quantum anomalous Hall effect, examined so far theoretically for Mn-doped HgTe QWs [38], could be observed in the Cr-doping case.

II. IMPURITY AND BAND STRUCTURE PARAMETER VALUES

A. Cr and Mn impurity levels

We place zero electron energy at the valence band top, $E_v = 0$. We are interested in three energy levels introduced by cation-substitutional Cr impurities in II-VI compounds (HgTe and ZnTe) and Mn impurities in GaN: (i) the donor level E_d corresponding to Cr $^{2+/3+}$ and Mn $^{3+/4+}$ states with the spin $S = 2$; (ii) two acceptor states of Cr $^{2+/1+}$ and Mn $^{3+/2+}$ located at energies $E_d + U$ and $E_d + U + J$ corresponding to five d electrons but different spin value, $S = 5/2$ and $S = 3/2$, respectively. The energies (E_d, U, J) are explicitly given in terms of Parmenter’s (E_0, U, J) in Sec. III (any reference to Parmenter’s notation is indicated explicitly). Spectroscopic free-ion data imply the exchange energy $J = 3$ eV [20]. For GaN:Mn we take $J = 2$ eV [25]. Experimental studies of ZnTe:Cr point to $E_d = 0.2$ eV and $U = 1.1$ eV [39]. Assuming the valence band offset between HgTe and ZnTe $W = 0.5$ eV, we anticipate $E_d = -0.3 \pm 0.1$ eV in HgTe:Cr. Similarly, experimental results for wz-GaN:Mn lead to $E_d = 1.1$ eV and $U = 0.7$ eV [40–42]. (In Ref. 25 $E_d = 1.8$ eV was incorrectly used). Because of the lack of reliable data for the internal strain parameter u , we assume that Cr and Mn impurities are located at the center of the tetrahedron of the nearest-neighbor anions; the distortion due to Jahn-Teller effect is neglected.

B. Tight-binding parameters

One of standard approaches to determine electronic energy bands in solids is the tight-binding approximation (TBA). Within that model, empirical or *ab initio* data provide on-site and overlap energies which serve to construct the Bloch Hamiltonian. We reuse the sp^3 band structure parameters given previously for HgTe [16]. to-

TABLE I. Summary of the electronic configurations involved in the leading order of perturbation theory for a d^4 ground state and spherical symmetry.

Configuration	Number of electrons	Spin (S)	Orbital angular momentum (L)	Energy (Parmenter)	Total degeneracy
d^3	3	3/2	1, 3	$3E_0 - 3J + 3U$	40
d^4	4	2	2	$4E_0 - 6J + 6U$	25
d^5	5	5/2	0	$5E_0 - 10J + 10U$	6
$d^{5\downarrow}$	5	3/2	1, 2, 3, 4	$5E_0 - 5J + 10U$	96

gether with $V_{pd\sigma} = -0.64$ eV, $V_{pd\pi} = -0.45V_{pd\sigma}$, and $V_{sd\sigma} = 1.08V_{ps\sigma}$ for Cr ions [20]. The tight-binding parameters of Ref. 43 are employed for ZnTe. For zb-GaN we reuse the parameter set of Ref. 25, whereas a set of parameters published by Yang *et al.* have been employed for wz-GaN, although we include all the second-neighbor overlaps (only half of them have been originally included). We neglect possible inconsistencies in the parameter set that may arise as a result.

In order to verify whether the present results are sensitive to details of the band-structure, additional models have been considered for (Hg,Cr)Te and (Zn,Cr)Te. These models include explicitly the d orbitals of both the cation and anion, thus allowing to include also d - d hybridization. In the band-structure models which include the d orbitals of the anion we assume for the hy-

bridization matrix elements, following the universal ratios of tight-binding overlaps [44]: $V_{dd\sigma} = -3.47$ eV, $V_{dd\pi} = 1.87$ eV, and $V_{dd\delta} = -0.51$ eV.

C. Splitting and shift of bands resulting from p - d hybridization

We begin our discussion of exchange interactions in our systems by introducing the second-order effective Hamiltonian for a band carrier coupled to a d^4 magnetic shell, including the effect of the p - d hybridization. The matrix elements between the initial and final configurations of a set of band states (denoted $\{k\}$) and the d^4 shell, in the occupation-number representation as $\{n_k\}$, are given by

$$\begin{aligned}
& \langle d_{fin}^4; \{n_{k;fin}\} | H_{eff}^{(2)} | d_{ini}^4; \{n_{k;ini}\} \rangle \\
&= \sum_{d_{int}^5; k, k'} A_{+1}(E_k, E_{k'}) \langle d_{fin}^4 | a_d(k') | d_{int}^5 \rangle \langle d_{int}^5 | a_d^\dagger(k) | d_{ini}^4 \rangle \langle \{n_{k;fin}\} | a_{k'}^\dagger a_k | \{n_{k;ini}\} \rangle + \\
&+ \sum_{d_{int}^5\downarrow; k, k'} A_{+1\downarrow}(E_k, E_{k'}) \langle d_{fin}^4 | a_d(k') | d_{int}^5\downarrow \rangle \langle d_{int}^5\downarrow | a_d^\dagger(k) | d_{ini}^4 \rangle \langle \{n_{k;fin}\} | a_{k'}^\dagger a_k | \{n_{k;ini}\} \rangle + \\
&+ \sum_{d_{int}^3; k, k'} A_{-1}(E_k, E_{k'}) \langle d_{fin}^4 | a_d^\dagger(k) | d_{int}^3 \rangle \langle d_{int}^3 | a_d(k') | d_{ini}^4 \rangle \langle \{n_{k;fin}\} | a_k a_{k'}^\dagger | \{n_{k;ini}\} \rangle, \quad (1)
\end{aligned}$$

where A_{+1} , $A_{+1\downarrow}$, and A_{-1} are temperature-dependent

numerical coefficients ($A_{+1\downarrow}$ is obtained from A_{+1} by the substitution $U \rightarrow U + J$):

$$\begin{aligned}
& A_{+1}(E_k, E_{k'}) \\
&= \frac{1}{(E_d + U - E_k)(E_d + U - E_{k'}) \left[\exp\left(\frac{E_k - E_d - U}{k_B T}\right) - \exp\left(\frac{E_{k'} - E_d - U}{k_B T}\right) \right]} \times \\
&\times \left[(E_d + U - E_{k'}) \exp\left(\frac{E_{k'} - E_d - U}{k_B T}\right) - (E_d + U - E_k) \exp\left(\frac{E_k - E_d - U}{k_B T}\right) + \right. \\
&\quad \left. + (E_{k'} - E_k) \exp\left(\frac{E_k - E_d - U}{k_B T}\right) \exp\left(\frac{E_{k'} - E_d - U}{k_B T}\right) \right], \tag{2}
\end{aligned}$$

$$\begin{aligned}
& A_{-1}(E_k, E_{k'}) \\
&= \frac{1}{(E_d - E_k)(E_d - E_{k'}) \left[\exp\left(\frac{E_k - E_d}{k_B T}\right) - \exp\left(\frac{E_{k'} - E_d}{k_B T}\right) \right]} \times \\
&\times \left[(E_d - E_{k'}) \exp\left(\frac{E_k - E_d}{k_B T}\right) - (E_d - E_k) \exp\left(\frac{E_{k'} - E_d}{k_B T}\right) + (E_{k'} - E_k) \right], \tag{3}
\end{aligned}$$

subspace	C	B
d^5	$\frac{1}{5}$	$\frac{2}{15}$
$d^{5\downarrow}$	$\frac{7}{15}$	$-\frac{7}{15}$
d^3	$\frac{1}{3}$	$\frac{1}{3}$

TABLE II. The numerical coefficients (matrix elements of the creation/annihilation operators) for p - d interaction of d orbitals of t_2 symmetry, averaged over the three Jahn-Teller configurations in order to restore the cubic symmetry. Notation: C is a spin-independent one-electron energy shift; B multiplies Heisenberg term $\mathbf{S} \cdot \mathbf{s}$.

which simplifies in the limit $T \rightarrow 0$, $\mu \rightarrow E_F$ to

$$A_{+1}(E_k, E_{k'}) = \frac{1}{\min(E_k, E_{k'}) - E_d - U}, \tag{4}$$

$$A_{-1}(E_k, E_{k'}) = \frac{1}{E_d - \max(E_k, E_{k'})} \tag{5}$$

under the assumptions $E_d < E_F$, $E_k, E_{k'} < E_d + U$.

The summation over an orthonormal set of intermediate states in each of the subspaces ($d_{int}^5, d_{int}^{5\downarrow}, d_{int}^4$) yields a one-particle hamiltonian for the band carrier. It is sensitive to the Jahn-Teller distortion of the magnetic impurity. At the Γ point, the carriers hybridize to t_2 orbitals only, and with the same strength V_{pd} to each of them. Now, averaging over the three Jahn-Teller configurations restores the cubic symmetry. In such circumstances the interaction assumes the form $C + B \mathbf{S} \cdot \mathbf{s}$, which is a constant one-particle energy (contributing to the band offset) plus the Heisenberg p - d exchange term. The numerical coefficients are summarized in Table II.

In the case of a conduction-band carrier, the symmetry allows also for an s - d term, originating from the potential exchange. Since the Bloch function for the conduction band is a mixture of both cation and anion orbitals, the corresponding exchange energy is reduced with respect to the free-ion.

III. THEORY OF SPIN-SPIN INTERACTIONS

We follow the established approach [16, 28, 31] based on the leading-order perturbation theory (4th-order in p - d hybridization). We use here the convention for the Hamiltonian representing spin pair interactions, $H_{ij} = -2J_{ij} \mathbf{S}_i \cdot \mathbf{S}_j$, where J_{ij} results from angular averaging to be discussed later, and — in general — contains three contributions, hh corresponding to superexchange, he describing the interband Bloembergen-Rowland coupling mechanism, and ee giving the two-electron contribution. We adapt here our previous theory [16] for the d^5 magnetic shells for the d^4 case.

The components of the full the Hamiltonian,

$$\hat{H} = (\hat{H}_k + \hat{H}_d) + \hat{V}_{\text{hyb}}, \tag{6}$$

correspond to a set of bands for non-interacting electrons ($\hat{H}_k = \sum_k E_k a_k^\dagger a_k$), the d -shells with the on-site Coulomb repulsion ($\hat{H}_d = \sum_i \hat{H}_{d,i}$, e.g., Parmenter's Hamiltonians [45]), and hybridization between the band states and the d -shells (\hat{V}_{hyb}). Application of the perturbation theory involves summing over processes in which the electron jumps from one d -shell (state d_1) to a band state (k), then to the d -shell of another magnetic ion (state d_2), then to another band state (k'), and then back to state d_1 — forming a closed path. Terms consisting of two independent loops (performed by two electrons) cancel in the total result. One has also to take into account, by means of the quasi-degenerate perturbation theory [46], that we are interested in the Hamiltonian just for the ground state of the two magnetic ions, $d^4 \otimes d^4$. Each term is a product of a phase due to the anticommutation rule for the fermionic creation and annihilation operators, an energetic denominator, and four matrix elements of the hybridization operator (the latter independent of the occupations of the band states or the order in which the transitions happen). We write the matrix elements of the effective Hamiltonian (between the initial and final states) as a sum over an orthonormal set

of intermediate states ($d_{int,1}, d_{int,2}$):

$$\begin{aligned}
& \left\langle d_{fin,1}, d_{fin,2} \left| H_{eff}^{(4)} \right| d_{ini,1}, d_{ini,2} \right\rangle \\
&= \sum_{k,k'} \sum_{d_{int,1}, d_{int,2}} A_{x_1, x_2}(E_k, E_{k'}, \mu) \\
&\quad \times \langle d_{fin,1} | a_{d,1, x_1}(k, k') | d_{int,1} \rangle \\
&\quad \times \langle d_{int,1} | a_{d,1, x_1}(k', k)^\dagger | d_{ini,1} \rangle \\
&\quad \times \langle d_{fin,2} | a_{d,2, x_2}(k', k) | d_{int,2} \rangle \\
&\quad \times \langle d_{int,2} | a_{d,2, x_2}(k, k')^\dagger | d_{ini,2} \rangle \quad (7)
\end{aligned}$$

Here, $x_i \in \{+1, -1\}$ is $+1$ for acceptor excitations (intermediate state $d_{int,i} \in d^5 \oplus d^{5\downarrow}$, see below) or -1 for donor excitations ($d_{int,i} \in d^3$), and $a_{d,i, x_i}(k, k')$ is an annihilation [$a_{d,i,+1}(k, k') = a_{d,i}(k)$] or creation [$a_{d,i,-1}(k, k') = a_{d,i}(k')^\dagger$] operator for the d -shell i , respectively. By definition, the hybridization operator can be written as the following sum over band states k :

$$\begin{aligned}
\hat{V}_{\text{hyb}} &= \sum_{i,k} [a_k^\dagger a_{d,i}(k) + a_{d,i}(k)^\dagger a_k], \quad (8) \\
a_{d,i}(k) &= \sum_{n,s,m} \langle k | n, s \rangle \langle n | V | d, i, m \rangle_{\kappa(k)} \\
&\quad \times e^{-i\kappa(k) \cdot \mathbf{R}_i} a_{d,i,m,s}, \quad (9)
\end{aligned}$$

where n is a band orbital index, $s \in \{\frac{1}{2}, -\frac{1}{2}\}$ is a spin index, m is a d -shell orbital index, and $\langle n | V | d, i, m \rangle_{\kappa(k)}$ is the tight-binding overlap [at the wave vector $\kappa(k)$ corresponding to band state k] between band orbital n and d -shell orbital m , the latter located at position \mathbf{r}_i inside the unit cell, and at absolute position $\mathbf{R}_i = n_1 \mathbf{a}_1 + n_2 \mathbf{a}_2 + n_3 \mathbf{a}_3 + \mathbf{r}_i$ [$(n_\alpha)_{\alpha=1,2,3}$ number lattice cells]. The phase factor $e^{-i\kappa(k) \cdot \mathbf{R}_i}$ compensates the fact that we are working with Bloch functions (rather than with wave functions).

The relevant subspace of the Hilbert space for the d -shells is a direct sum of the subspaces corresponding to the electronic configurations being involved in the leading order: d^4 (ground state), d^3 , d^5 (high-spin) and $d^{5\downarrow}$

(spin-flipped). Since even in a tetrahedral symmetry this amounts to a 32-parameter Hamiltonian, we are virtually forced to reuse the three-parameter Hamiltonian of Parmenter [45]. The relevant energies are given in terms of Parmenter's E_0 , U , J in Table I. We will denote as $E_d - E_v$, $E_d + U - E_v$, and $E_d + U + J - E_v$ the energies of the transitions $d^3 \rightarrow d^4 + h$, $d^4 \rightarrow d^5 + h$, $d^4 \rightarrow d^{5\downarrow} + h$ (respectively; h stands for a hole at the valence-band top, and E_v for the valence-band-top energy). The parameters E_d , U , and J adopted in the present Article are related to the original Parmenter's parameters E_0 , U , and J according to: $E_d \rightarrow E_0 + 3(U - J)$, $U \rightarrow (U - J)$, $J \rightarrow 5J$, where the r.h.s. is expressed in terms of Parmenter's (E_0, U, J).

Explicit expressions for A 's (including the phase factors) can be written for d^3 and d^5 excitations in an insulator ($E_k < E_F$ or $E_k > E_F$) in the low-temperature

TABLE III. A summary of the reduced matrix elements for the d -shells annihilation operators; cf. Eqs. (16–17).

n	S	L	S'	L'	$ \langle\langle a \rangle\rangle_{L,S;L',S'} ^2$
3	3/2	1	2	2	6/5
3	3/2	3	2	2	14/5
4	2	2	5/2	0	5
4	2	2	3/2	1	5/4
4	2	2	3/2	2	5/4
4	2	2	3/2	3	5/4
4	2	2	3/2	4	5/4

limit, $T \rightarrow 0^+$, $\mu \rightarrow E_F$, $f(E_k) \rightarrow \Theta(E_F - E_k)$, under the assumption that the ground state of the unperturbed Hamiltonian ($H_k + H_d$) corresponds to d^4 electronic configuration, i.e., $E_d < E_F$, $E_d + U > E_F$, and $E_d + U + J > E_F$ (the expression for $d^{5\downarrow}$ excitations are obtained by replacing U with $U + J$ for the corresponding shell d_i ; zero denominators, e.g. $E_{d,1} - E_{d,2}$, must be eliminated by taking appropriate limits: $E_{d,1}, E_{d,2} \rightarrow E_d$, and/or formal algebraic transformations).

$$\begin{aligned}
A_{+1,+1} &= \frac{1}{2} \frac{f(E_k) - f(E_{k'})}{E_k - E_{k'}} [w_{1u}(E_k)w_{2u}(E_k) + w_{1u}(E_{k'})w_{2u}(E_{k'})] + \\
&\quad - \frac{1}{2} [f(E_k) + f(E_{k'})] \frac{w_{1u}(E_k)w_{1u}(E_{k'}) - w_{2u}(E_k)w_{2u}(E_{k'})}{E_{d1} + U_1 - E_{d2} - U_2} \quad (10)
\end{aligned}$$

$$\begin{aligned}
A_{+1,-1} &= \frac{1}{2} \frac{f(E_k) - f(E_{k'})}{E_k - E_{k'}} [w_{1u}(E_k)w_2(E_k) + w_{1u}(E_{k'})w_2(E_{k'})] + \\
&\quad - \frac{1}{2} [f(E_k) + f(E_{k'})] \frac{w_{1u}(E_k)w_{1u}(E_{k'}) - w_2(E_k)w_2(E_{k'})}{E_{d1} + U_1 - E_{d2}} + \\
&\quad - \frac{w_2(E_k)w_2(E_{k'})}{E_{d1} + U_1 - E_{d2}} \quad (11)
\end{aligned}$$

$$\begin{aligned}
A_{-1,+1} &= \frac{1}{2} \frac{f(E_k) - f(E_{k'})}{E_k - E_{k'}} [w_1(E_k)w_{2u}(E_k) + w_1(E_{k'})w_{2u}(E_{k'})] + \\
&\quad - \frac{1}{2} [f(E_k) + f(E_{k'})] \frac{w_1(E_k)w_1(E_{k'}) - w_{2u}(E_k)w_{2u}(E_{k'})}{E_{d1} - E_{d2} - U_2} + \\
&\quad + \frac{w_1(E_k)w_1(E_{k'})}{E_{d1} - E_{d2} - U_2}
\end{aligned} \tag{12}$$

$$\begin{aligned}
A_{-1,-1} &= \frac{1}{2} \frac{f(E_k) - f(E_{k'})}{E_k - E_{k'}} [w_1(E_k)w_2(E_k) + w_1(E_{k'})w_2(E_{k'})] + \\
&\quad - \frac{1}{2} [f(E_k) + f(E_{k'})] \frac{w_1(E_k)w_1(E_{k'}) - w_2(E_k)w_2(E_{k'})}{E_{d1} - E_{d2}} + \\
&\quad + \frac{w_1(E_k)w_1(E_{k'}) - w_2(E_k)w_2(E_{k'})}{E_{d1} - E_{d2}}
\end{aligned} \tag{13}$$

$$w_i(E) = \frac{1}{E_{di} - E} \tag{14}$$

$$w_{iu}(E) = \frac{1}{E_{di} + U_i - E} \tag{15}$$

Matrix elements of the annihilation operators from

d^{n+1} to d^n can be written in terms of Clebsch-Gordan coefficients as:

$$\begin{aligned}
\langle d^n, \alpha, L, S, L_{z,f}, S_{z,f} | a_{L_{z,a}, S_{z,a}} | d^{n+1}, \beta, L', S', L_{z,i}, S_{z,i} \rangle = \\
\langle \langle a \rangle \rangle_{\alpha, L, S; \beta, L', S'} \langle L', L_{z,i} | L, L_{z,f}; 2, L_{z,a} \rangle \left\langle S', S_{z,i} \left| S, S_{z,f}; \frac{1}{2}, S_{z,a} \right. \right\rangle,
\end{aligned} \tag{16}$$

where $(L_{z,a}, S_{z,a})$ are the quantum numbers of the an-

ihilated electron. Analogously, we have for matrix elements of the creation operators from d^n to d^{n+1} :

$$\begin{aligned}
\langle d^{n+1}, \alpha, L, S, L_{z,f}, S_{z,f} | a_{L_{z,c}, S_{z,c}}^\dagger | d^n, \beta, L', S', L_{z,i}, S_{z,i} \rangle = \\
\langle \langle a^\dagger \rangle \rangle_{\alpha, L, S; \beta, L', S'} \langle L, L_{z,f} | L', L_{z,i}; 2, L_{z,c} \rangle \left\langle S, S_{z,f} \left| S', S_{z,i}; \frac{1}{2}, S_{z,c} \right. \right\rangle,
\end{aligned} \tag{17}$$

with $\langle \langle a^\dagger \rangle \rangle_{\alpha, L, S; \beta, L', S'} = \langle \langle a \rangle \rangle_{\beta, L', S'; \alpha, L, S}^*$. The squared absolute values of the reduced matrix elements are summarized in Table III.

We further restrict our attention to the case when the orbital configurations m_i of the d -shells remain unchanged. In such a situation an excitation (electron or hole) which enters the d -shell with an orbital quantum number m , leaves it with m unchanged. Then, the spin-

dependent parts of the subexpressions

$$\begin{aligned}
\sum_{d_{int,i} \in d_{sub,i}} \langle d_{fin,i} | a_{d,i,m,s} | d_{int,i} \rangle \langle d_{int,i} | a_{d,i,m,s'}^\dagger | d_{ini,i} \rangle \\
\cong j_{m,m_i}(d_{sub,i}) \sum_{\alpha} \langle d_{fin,i} | S_{i,\alpha} | d_{ini,i} \rangle \langle s | \sigma_{\alpha} | s' \rangle,
\end{aligned} \tag{18}$$

$$\begin{aligned}
\sum_{d_{int,i} \in d_{sub,i}} \langle d_{fin,i} | a_{d,i,m,s}^\dagger | d_{int,i} \rangle \langle d_{int,i} | a_{d,i,m,s'} | d_{ini,i} \rangle \\
\cong j_{m,m_i}(d_{sub,i}) \sum_{\alpha} \langle d_{fin,i} | S_{i,\alpha} | d_{ini,i} \rangle \langle s' | \sigma_{\alpha} | s \rangle,
\end{aligned} \tag{19}$$

TABLE IV. Values of $j_{m,m_i}(d_{sub,i})$ in equations (18) and (19) for an excitation with an orbital quantum number m from a d^4 ground state with an orbital configuration m_i (rows correspond to sectors of the Hilbert space) under spherical symmetry.

$d_{sub,i}$	$ m = m_i \quad m \neq m_i$	
d^3	0	1/4
d^5	1/5	0
$d^{5\downarrow}$	-1/5	-1/4

and $j_{m,m_i}(d_{sub,i})$ are constant numbers which depend on the Hilbert subspace, $d_{sub,i}$, and the relation between the orbital quantum number m and the orbital state of the d -shell, m_i , as summarized in Table IV.

Equipped with the results (10–13) and Table IV, we rederive Eqs. 1–9 of Ref. 20. In Ref. 20, the contribution with $m \neq m_i$ at both ions ($i = 1, 2$) is denoted F ; that with $m = m_i$ at both ions is denoted G ; the remaining contribution is denoted H . One therefore has [20, Eq. 2]

$$J_{\alpha\beta}^{\gamma\delta}(\mathbf{R}_{12}) = F_{\alpha\beta}^{\gamma\delta}(\mathbf{R}_{12}) + H_{\alpha\beta}^{\gamma\delta}(\mathbf{R}_{12}) + G_{\alpha\beta}^{\gamma\delta}(\mathbf{R}_{12}). \quad (20)$$

We let $f(E_k), f(E_{k'}) \rightarrow 1$ in our (10–13) and find dif-

$$\begin{aligned} & \frac{1}{E_d + U + J - E_k} \frac{1}{E_d + U + J - E_{k'}} \left(\frac{2}{U + J} + \frac{1}{E_d + U + J - E_k} + \frac{1}{E_d + U + J - E_{k'}} \right) \\ &= \begin{bmatrix} \left(2 + \frac{U+J}{E_d+U+J-E_{k'}} \right) \frac{U+J}{E_d+U+J-E_{k'}} \\ \left(\frac{U+J}{E_d+U+J-E_{k'}} \right)^2 \end{bmatrix}^T \begin{bmatrix} \frac{1}{2(U+J)^3} & 0 \\ 0 & -\frac{1}{2(U+J)^3} \end{bmatrix} \begin{bmatrix} \left(2 + \frac{U+J}{E_d+U+J-E_k} \right) \frac{U+J}{E_d+U+J-E_k} \\ \left(\frac{U+J}{E_d+U+J-E_k} \right)^2 \end{bmatrix}, \quad (21) \end{aligned}$$

which resembles LDU decomposition of some matrix. In this form, the dependence on E_k has been separated from that on $E_{k'}$. Therefore, one can group this energy dependence in the product with the hybridization matrix elements; then the multiplication by the remaining plane wave phase factor and summation over momentum is just a Fourier transform (and it can be performed by means of the FFT algorithm). In this way we obtain the whole real-space dependence of the spin-spin Hamiltonian in one turn, where the algorithm loops over the diagonal of the matrix D above. The most difficult part here is the he term, which features an $E_k - E_{k'}$ denominator; we handle it by performing an incremental on-the-fly LDU decomposition of the matrix $(1/(E_k - E_{k'}))_{k,k'}$, which yields D of the size $\min(n_v, n_c)$ (the number of valence or conduction band states, whichever is lower).

Another challenge in the double integration over the Brillouin zone, in the case of the interband he term in zero-gap HgTe, is the singularity that appears at $k, k' \rightarrow 0$. We follow the procedure elaborated previously [16], which involves a shift of the k grid by different ϑ values.

ferences w.r.t. Ref. 20: an incorrect normalization (the prefactor 2 in Eq. 1 of Ref. 20 is extraneous), wrong signs of \mathcal{F} and \mathcal{H} , a missing 2 in the numerator of $1/(e_2 + e_1)$ in \mathcal{F} , and a lacking symmetrization of \mathcal{H} with respect to $\nu \leftrightarrow \nu'$ (the last issue does not affect numerical values). Still, the numbers (e.g. for ZnTe:Cr) in Table I of Ref. 20 are $-1/2$ the values that can be obtained from the incorrect formulas. However, as shown in the next section, those corrections to the hh contribution, together with he and ee terms taken into account here but neglect previously, while important quantitatively, do not alter the main conclusion of the previous works [20, 25]: spin-spin interactions are predominately FM for magnetic ions with high spin d^4 configuration in zinc-blende DMSs.

Even though the energy shifts due to Jahn-Teller effect are not taken into account in the present theory, the exchange integrals are sensitive to orbital configurations. We report as J its average over the three T_2 states of each of the two d -shells in question (with an appropriate transformation of the quantization axis in the wurtzite case, as described in Appendix A).

For practical and efficient numerical evaluation of the double Brillouin zone integral, it is desirable to perform one more algebraic transformation at this stage. We take \mathcal{F} with $f(E_k), f(E_{k'}) \rightarrow 1$ as an example, and write

The number of k and ϑ values employed here insures convergence of the results.

As an ending remark, the fourth order perturbation to the Hamiltonian for a pair of transition metal impurities, after averaging over orbitals and neglecting the spin-orbit interaction, assumes the Heisenberg form. This is so because the electron's spin $s = 1/2$ in the underlying theory; however, other forms beyond the approach implemented here — like biquadratic or four-spin couplings — are possible and can be found by examining ab initio the dependence of the system energy on the q -vector of a frozen magnon, as pioneered by Liechtensten et al. [47].

IV. NUMERICAL VALUES OF THE EXCHANGE INTEGRALS

We report our results in the convention according to which the Hamiltonian H_{ij} for a pair (i, j) is

$$H_{ij} = -2J_{ij} \mathbf{S}_i \cdot \mathbf{S}_j, \quad (22)$$

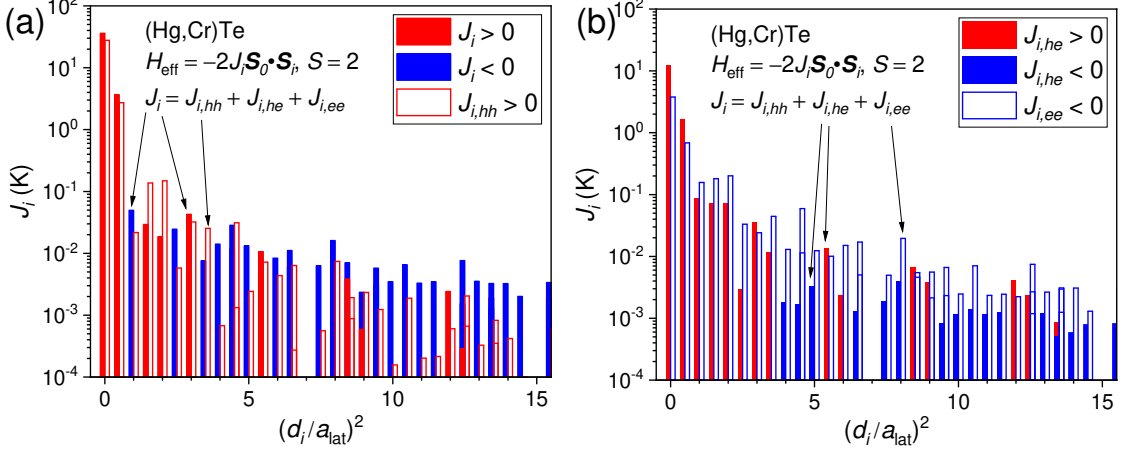


FIG. 1. Exchange integrals J_i in a logarithmic scale for spin pairs at distances d_i corresponding to the first thirty cation coordination spheres $1 \leq i \leq 30$, $d_i = (i/2)^{1/2} a_{\text{lat}}$ in zinc-blende topological (Hg,Cr)Te. (a) The total exchange energies and the superexchange (hh) contribution; (b) the remaining contributions: the electron-hole (Bloembergen-Rowland) and two-electron terms (he and ee , respectively). Red and blue colors correspond to the FM and AFM sign of the interaction, respectively. As demonstrated elsewhere in the context of (Hg,Mn)Te [16], the self-interaction terms at $d_i = 0$ do not contribute to spin-spin exchange energies but account for a sizable overestimation of the interband contribution he to the Curie temperature T_C , if evaluated in terms of the interband Van Vleck susceptibility [5].

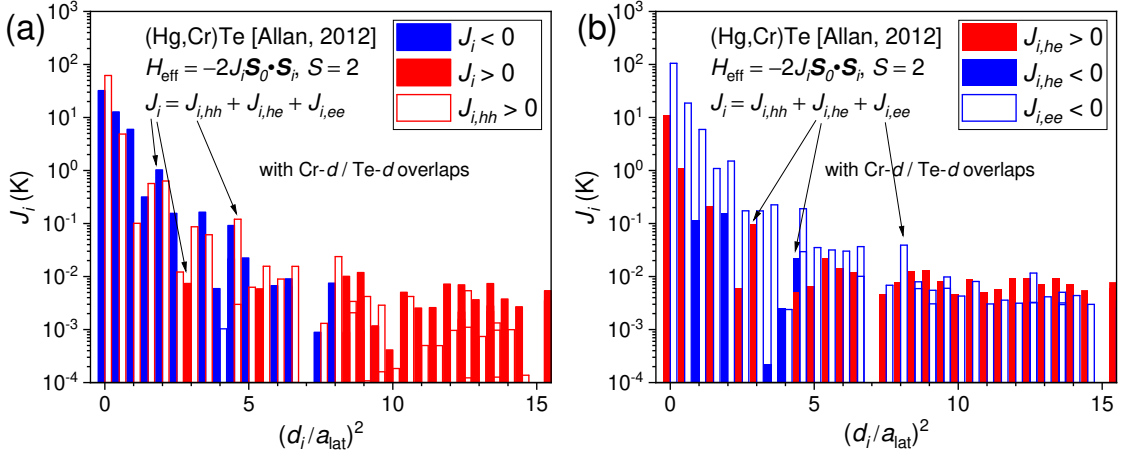


FIG. 2. Exchange integrals J_i in zinc-blende topological (Hg,Cr)Te according to the band-structure model of Ref. 48 (2048 k -points, 64 θ -points).

where \mathbf{S}_i and \mathbf{S}_j are the quantum operators for $S = 2$ spins. We present, in Figs. 1– 5 for (Hg,Cr)Te, (Zn,Cr)Te, and zb-(Ga,Mn)N, respectively the determined values of $J_{ij} \equiv J_i$ vs. the spin pair distance $R_{ij} \equiv d_i$, where $d_i = (i/\sqrt{2})a_{\text{lat}}$ denote the positions of the sequential cation coordination spheres and the lattice parameters $a_{\text{lat}} = 0.646$ and 0.610 nm for HgTe and ZnTe, respectively. Since the magnitudes of J_{ij} decay exponentially with d_i , only the first few J_{ij} values are significant and, therefore, shown in Tables V–VIII for

the same systems and wz-(Ga,Mn)N.

Another relevant quantity is the Curie-Weiss parameter,

$$\Theta_0 = \frac{2}{3} \sum_{i \geq 1} z_i J_i S(S+1), \quad (23)$$

where z_i is the number of cations in the i -th coordination sphere. In terms of Θ_0 and according to the high-temperature expansion [50], Curie-Weiss temperature [equal to Curie temperature T_C in the mean-field

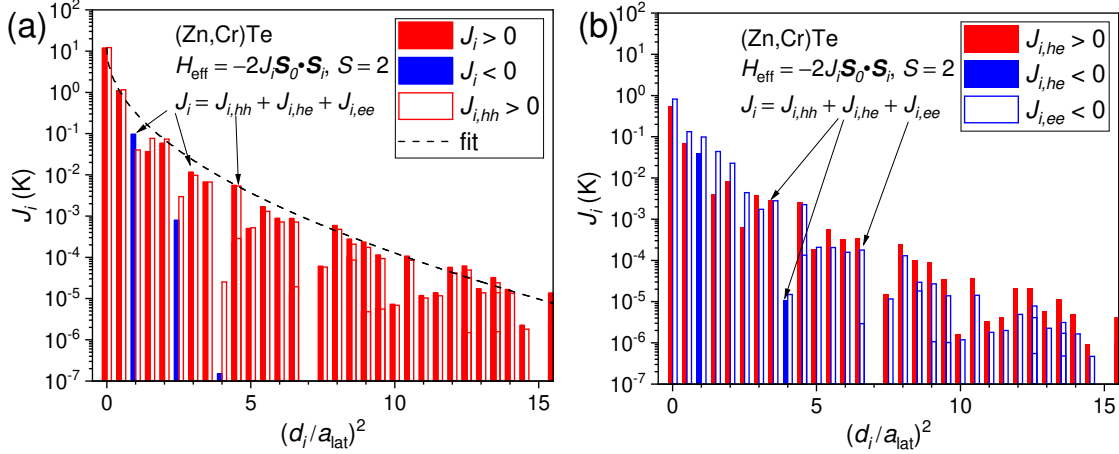


FIG. 3. Same as in Fig.1 but for topologically trivial zinc-blende (Zn,Cr)Te.

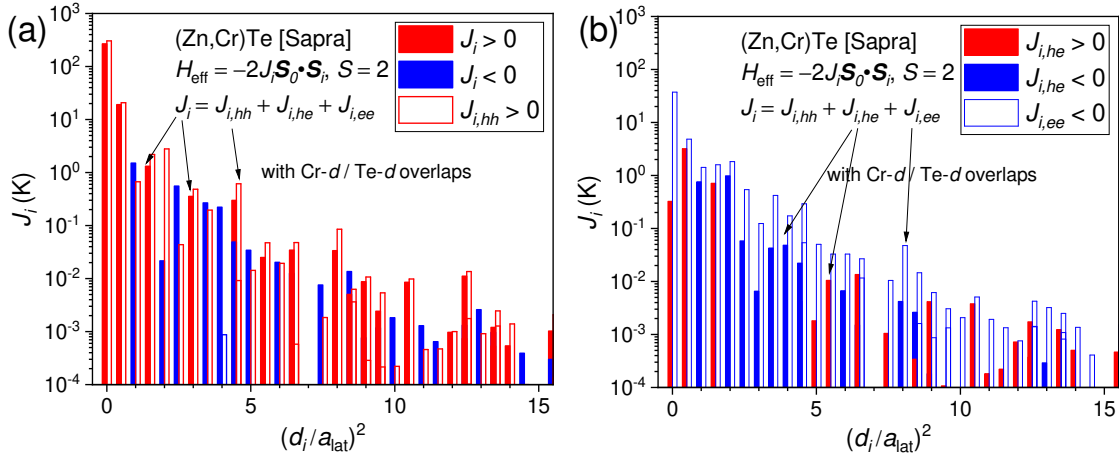


FIG. 4. Exchange integrals J_i in zinc-blende topologically trivial (Zn,Cr)Te according to the band-structure model of Ref. 49 (without second neighbor interactions; 16384 k -points).

approximation (MFA)], is given by $\Theta_{CW} = x\Theta_0$, if a dependence of the band structure parameters on fractional magnetic cation content x can be neglected. The values of Θ_{CW} for $x = 0.1$ are shown in Table IX for the studied systems.

Several conclusions emerge from the results displayed in Figs. 1–6 and Tables V–IX. First, as shown previously [16], within the Van Vleck susceptibility model [5], $T_C^{(VV)} = x\Theta_0^{(VV)}$, where $\Theta_0^{(VV)}$ involves the summation only over $J_{i,he}$ and includes the self-interaction $J_{0,he}$ term with $z_0 = 1$. Since this spurious $J_{0,he}$ term is quite large, its inclusion with a simultaneous disregarding of superexchange (the hh term), leads to the improper conclusion about the dominant role of the Van Vleck mechanism. Second, judging from the Θ_0 values, FM interactions are

about an order of magnitude stronger in both zb- and wz-(Ga,Mn)N compared to (Hg,Cr)Te and (Zn,Cr)Te. Within our model, this fact results from a short lattice constant of GaN leading to sizable pd hybridization and a rather large magnitude of J_1 , as found by *ab initio* studies and experimentally [51]. Third, AFM ee term is surprisingly large in the case of (Hg,Cr)Te and (Zn,Cr)Te pointing to a possible competition between spin-glass and FM ordering at low temperatures in those systems. The presence of two competing terms indicates that theoretical conclusions on the magnetic ground state and corresponding ordering temperature may sensitively depend on the assumed values of the d -shell energies (E_d, U, J) and tight-binding parameters. The computations performed for two tight-binding models presented in Figs. 1–4 for (Hg,Cr)Te and (Zn,Cr)Te confirm such a strong

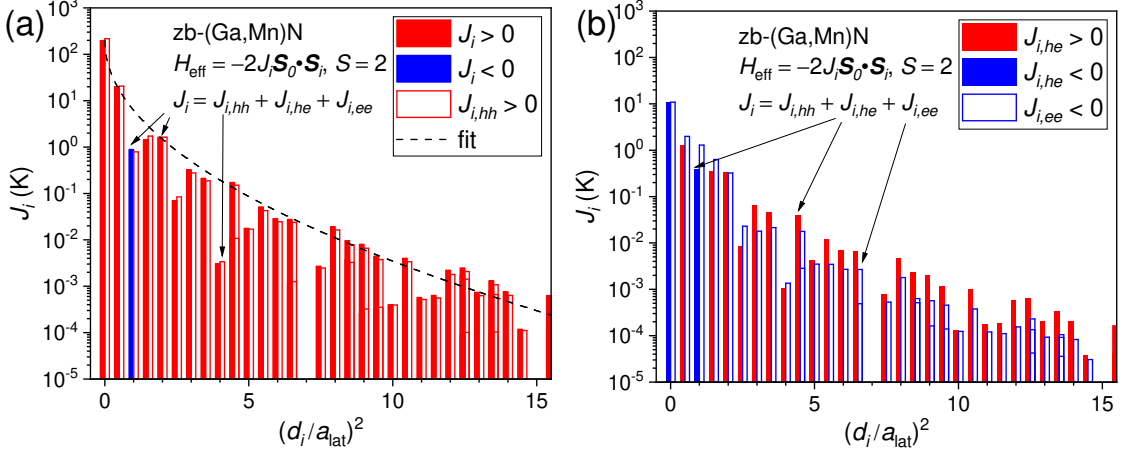


FIG. 5. Same as in Fig.1 but for topologically trivial zinc-blende (Ga,Mn)N.

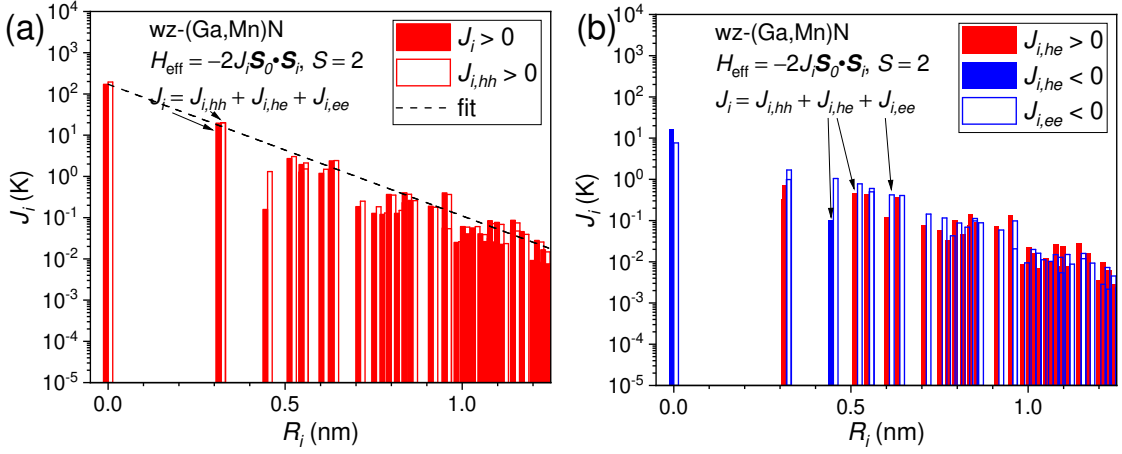


FIG. 6. Exchange integrals J_i in a logarithmic scale for spin pairs at distances $R_i < 1$ nm in topologically-trivial wurtzite (Ga,Mn)N. See the caption of Fig.1 for the legend.

sensitivity of J_i to details of the band-structure representation, and indicate importance of the hybridization between the magnetic d -shells of Cr and the d orbitals of Te.

In the situation outlined above, the results of recent first principles computations, carried out for (Hg,Cr)Te and (Cd,Cr)Te [52] using the hybrid functional approach, are particularly relevant. Surprisingly, those data have demonstrated a dependence of the interaction sign on the setting of the functional mixing parameter a_{HSE} : the interaction tended to be FM in (Hg,Cr)Te for $a_{\text{HSE}} = 0.5$, but AFM for $a_{\text{HSE}} = 0.32$ and 0.25 . Altogether, both tight-binding and ab initio results point to the fact that spin-spin coupling in (Hg,Cr)Te is on the borderline between FM and AFM regime, which opens a door for magnetism manipulations by e.g. strain, pressure and

electric field.

V. CURIE TEMPERATURES FROM MONTE CARLO SIMULATIONS AND PERCOLATION THEORY

Issues that can be encountered while attempting to find, by means of Monte Carlo simulations, the Curie temperature of a site-diluted system, were recollected elsewhere [53]. We assume that a fraction ($x = 0.1$) of randomly-chosen cation sites are occupied by local spins, represented in the simulation by unit vectors \mathbf{m}_i and pairwise coupled by isotropic Heisenberg interaction with $S(2S+1)J_{ij}$, where $S = 2$ and J_{ij} values are given in Tables V–VIII. In the zinc-blende case, we limit the interac-

TABLE V. (Hg,Cr)Te: Numerical values of the total pair exchange integrals J_i and contributions hh , he , and ee for the nearest cation coordination zones located at distances $d_i = \sqrt{i/2}a_{\text{lat}}$ and containing z_i cations. Positive and negative signs of J correspond to FM and AFM coupling, respectively. The computations have been performed for 16384 k -points and 512 θ -points (see, Sec. III and Ref. 16).

i	$J_i(\text{K})$	$J_{i,hh}(\text{K})$	$J_{i,he}(\text{K})$	$J_{i,ee}(\text{K})$	z_i
1	3.6631	2.7219	1.6255	-0.6843	12
2	-0.0496	0.0217	0.0857	-0.1570	6
3	0.0292	0.1371	0.0730	-0.1809	24
4	0.0185	0.1489	0.0707	-0.2011	12

TABLE VI. Same as in Table V but for zb-(Zn,Cr)Te (16384 k -points).

i	$J_i(\text{K})$	$J_{i,hh}(\text{K})$	$J_{i,he}(\text{K})$	$J_{i,ee}(\text{K})$	z_i
1	1.0936	1.1579	0.0687	-0.1330	12
2	-0.0967	0.0402	-0.0384	-0.0985	6
3	0.0366	0.0765	0.0040	-0.0438	24
4	0.0588	0.0734	0.0082	-0.0228	12

tion to the neighbor pairs at the distance $R_{ij} \leq 2\sqrt{2}a_{\text{lat}}$; in the wurtzite variant, $R_{ij} \leq 1.0$ nm.

Periodic boundary conditions have been assumed, and — for the smallest simulated sizes — the couplings with images of each spin in neighboring supercells are included by summing within the truncation distance. System sizes range from $L = 4$ (256 disorder realizations) to $L = 24$ (16 disorder realizations). In the wurtzite case, the proportions of the lattice block are 3:3:2 (and L refers to the linear system size along the c -axis). The numbers of temperatures in the simulation is kept constant at $N_T = 24$. For each realization, 4+4 burnin/measurement cycles are performed, with the number of Monte Carlo steps in each cycle increasing linearly with the linear system size, starting at 2000 steps ($L = 4$).

Figures 7 and 8 present examples of temperature dependencies of magnetization square $[\langle \mathbf{m} \rangle^2]$ and the modified Binder cumulant for disordered magnetic systems [53],

$$V_4\{m\} = \frac{1}{2} \frac{[5\langle \mathbf{m}^2 \rangle^2 - 3\langle \mathbf{m}^4 \rangle]}{[\langle \mathbf{m}^2 \rangle^2]}, \quad (24)$$

TABLE VII. Same as in Table V but for zb-(Ga,Mn)N (16384 k -points).

i	$J_i(\text{K})$	$J_{i,hh}(\text{K})$	$J_{i,he}(\text{K})$	$J_{i,ee}(\text{K})$	z_i
1	19.879	20.579	1.289	-1.989	12
2	-0.884	0.788	-0.386	-1.286	6
3	1.440	1.725	0.345	-0.630	24
4	1.629	1.625	0.326	-0.321	12

TABLE VIII. Same as Table V but for wz-(Ga,Mn)N (1152 k -points per unit cell of the reciprocal lattice).

i	$R_i(\text{\AA})$	$J_i(\text{K})$	$J_{i,hh}(\text{K})$	$J_{i,he}(\text{K})$	$J_{i,ee}(\text{K})$	z_i
1	3.180	19.498	20.166	0.325	-0.988	6
2	3.189	18.898	19.859	0.729	-1.690	6
3	4.503	0.158	1.309	-0.101	-1.050	6
4	5.185	2.704	3.034	0.449	-0.779	2
5	5.518	1.272	1.519	0.250	-0.497	12
6	5.524	1.944	2.113	0.430	-0.599	6
7	6.087	1.186	1.487	0.120	-0.421	12
8	6.378	2.376	2.420	0.361	-0.405	6

TABLE IX. Curie-Weiss temperatures Θ_{CW} equivalent to Curie temperatures T_{C} within the mean-field approximation compared to T_{C} values obtained by Monte-Carlo (MC) simulations and the percolation (perc) theory (see Sec. V) for the systems under study with 10% cations substituted by magnetic impurities.

compound	$\Theta_{\text{CW}}(\text{K})$	$T_{\text{C}}^{\text{MC}}(\text{K})$	$T_{\text{C}}^{\text{perc}}(\text{K})$
zb-Hg _{0.9} Cr _{0.1} Te	15.3	—	—
zb-Hg _{0.9} Cr _{0.1} Te [Allan]	-86.0	—	—
zb-Zn _{0.9} Cr _{0.1} Te	5.90	0.75	1.50
zb-Zn _{0.9} Cr _{0.1} Te [Sapra]	92.0	—	—
zb-Ga _{0.9} Mn _{0.1} N	123.8	28	30.1
wz-Ga _{0.9} Mn _{0.1} N	129.1	32	31.3

obtained by Monte-Carlo simulations for zb-Ga_{0.9}Mn_{0.1}N with various system sizes L . Here, the square brackets denote an average over disorder realizations. The crossing point of $V_4\{m\}$ curves determines Curie temperature T_{C} . The same procedure has been successful in the case of wz-Ga_{0.9}Mn_{0.1}N and zb-Zn_{0.9}Cr_{0.1}Te, and the obtained T_{C} values are displayed in Table IX. However, because of competitions between ferromagnetic and antiferromagnetic interactions, as shown in Fig. 1, Monte Carlo simulations have not been conclusive for zb-Hg_{0.9}Cr_{0.1}Te, pointing to a possibility of spin-glass freezing in that system.

It is interesting to compare the Monte-Carlo results to the expectations of the MFA and percolation theory for dilute ferromagnetic systems. For instance, in the case of zinc-blende Ga_{0.9}Mn_{0.1}N, according to Table IX $T_{\text{C}}^{\text{MFA}} = 124$ K, whereas $T_{\text{C}}^{\text{MC}} = 28$ K. This significant difference was already noted in the context of *ab initio* studies of DFSs with short-range exchange interactions [33]. However, in the case of, for instance (Ga,Mn)As, where long range carrier-mediated interactions dominate, the difference between $T_{\text{C}}^{\text{MFA}}$ and T_{C}^{MC} is much smaller, typically below 50% [54].

The percolation theory [32] was developed for continuous systems with exchange coupling $J(r)$ decaying exponentially with the spin pair distance r ,

$$J(r) = J_0 \exp(-r/b), \quad (25)$$

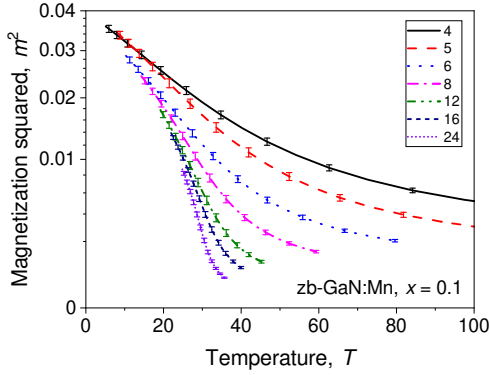


FIG. 7. Examples of temperature dependence of magnetization square in $\text{zb-Ga}_{1-x}\text{Mn}_x\text{N}$, $x = 0.1$ obtained by the Monte-Carlo simulations.

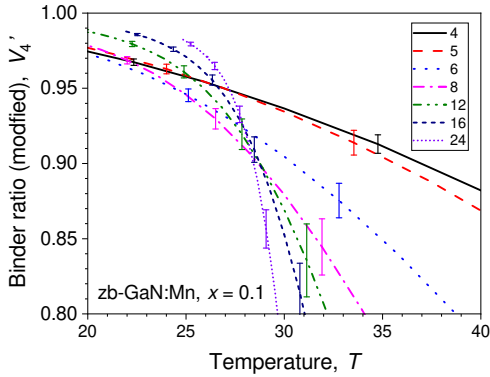


FIG. 8. Examples of temperature dependencies of the modified Binder ratio for $\text{zb-Ga}_{1-x}\text{Mn}_x\text{N}$, $x = 0.1$ obtained by Monte-Carlo simulations.

for which T_C can be written in the form [32],

$$T_C^{\text{perc}} \approx [S(2S + 1)]J_0 \exp\left(-\frac{0.89}{b(xN_0)^{1/3}}\right), \quad (26)$$

where N_0 is the cation concentration of magnetic ions. The values of T_C computed with these parameters and (26) are shown in Fig. 9 as a function of x in comparison to the Monte Carlo and experimental results.

By fitting Eq. 25 to J_i data displayed in Figs. 3, 5, and 6 we obtain, $J_0 \approx 12.0, 197, 172$ K and $b \approx 0.168, 0.130,$ and 0.136 nm for zb-(Zn,Cr)Te , zb-(Ga,Mn)N , and wz-(Ga,Mn)N , respectively. We omit fitting the data for $(\text{Hg,Cr)Te}$, as a departure from (25) is evident from oscillations of J . Similarly, we were unsuccessful fitting the alternative $J(r)$ for $(\text{Zn,Cr)Te}$ (Fig. 4). As shown in Table IX, the resulting magnitudes of T_C^{perc} agree with the T_C values determined by Monte-Carlo simulations in both zb-(Ga,Mn)N and wz-(Ga,Mn)N . This agreement allows us to evaluate $T_C(x)$ from the percolation formula (26), avoiding computationally expensive Monte-Carlo simulations for many x values and disorder realizations. In Fig. 9, the values of $T_C(x)$ we have obtained in this way are compared to experimental data [17, 22–24] and

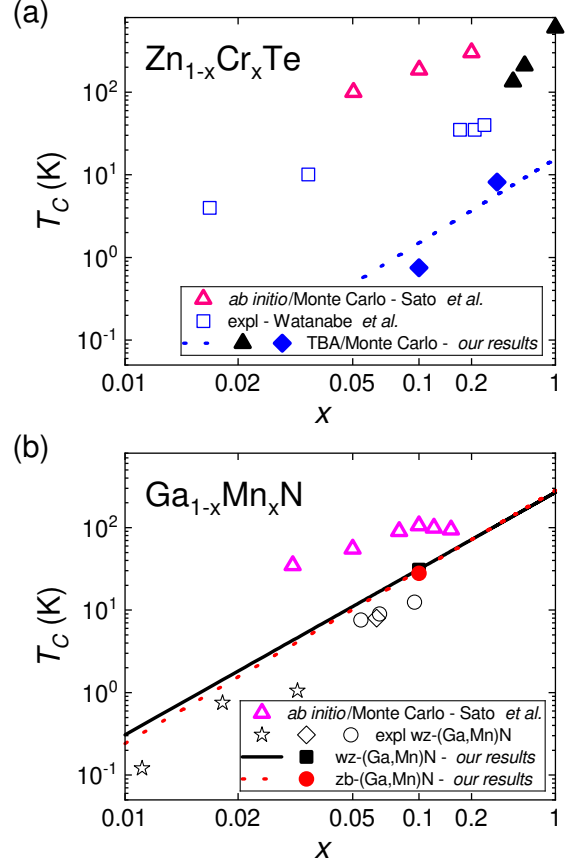


FIG. 9. Curie temperatures T_C in (a) $\text{Zn}_{1-x}\text{Cr}_x\text{Te}$ and (b) $\text{Ga}_{1-x}\text{Mn}_x\text{N}$. Present results are shown by solid points obtained by tight-binding computations (Figs. 3–6) and Monte Carlo simulations. The fits of $J(r)$ served to determine $T_C(x)$ from the percolation theory, as shown by dotted and solid lines for zinc-blende and wurtzite systems, respectively. Solid triangles: alternative parameterization data (Fig. 4). Hollow triangles: previous *ab initio* and Monte Carlo results [33]; experimental data: squares [17], diamond [22], stars [23], circles [24].

earlier *ab initio* results [33]. As seen, the present theory predicts much smaller values of T_C than the *ab initio* method which, within the local functional approximation, underestimates the localization degree of transition metal d orbitals in semiconductors. Our T_C values are lower than experimental points in the case of $\text{Zn}_{1-x}\text{Cr}_x\text{Te}$ at low x , which may point out to some aggregation of Cr ions in the studied layers, sensitivity to band-structure modelling, or significance of the departure from (25).

VI. *sp-d* EXCHANGE INTEGRALS AND THE QUANTUM TOPOLOGICAL HALL EFFECTS

In tetrahedrally coordinated DMSs, exchange coupling between band carriers near the Brillouin zone center and

cation-substitutional magnetic ions, $\mathcal{H}_{sp-d}^{(i)} = -\mathcal{J}\mathbf{s} \cdot \mathbf{S}_i$, is described by two exchange integrals [30], $\alpha = \langle S|\mathcal{J}|S\rangle$ and $\beta = \langle X|\mathcal{J}|X\rangle$, where here S and X are the periodic part of the Bloch functions (Kohn-Luttinger amplitudes) that transform as atomic s and p_x wave functions under the point symmetry group operations. Typically, α and β originate from the FM intra-atomic s - d potential exchange and the p - d hybridization, respectively. Furthermore, in many cases the molecular-field and virtual-crystal approximations hold allowing a straightforward determination of α and β from band splittings once macroscopic magnetization is known.

Making use of *NIST Atomic Spectra Database Levels*, we obtain $\mathcal{J}_{4s-3d} = 0.372$ eV for Cr^{1+} ions, which constitutes an upper limit for the exchange energy $N_0\alpha$ in Cr-doped compounds. For comparison, $\mathcal{J}_{4s-3d} = 0.391$ eV for Mn^{1+} , close to experimental [55, 56] and *ab initio* [57] values for (Hg,Mn)Te, $N_0\alpha = 0.4 \pm 0.1$ and 0.35 ± 0.05 eV, respectively. In view of this discussion, we expect

$$N_0\alpha = 0.3 \pm 0.1 \text{ eV} \quad (27)$$

for $\text{Hg}_{1-x}\text{Cr}_x\text{Te}$.

However, in the case of wide-gap II-VI Mn-contained DMSs, in which the conduction-band wave function becomes significantly spread on anions, $N_0\alpha$ values are much reduced, e.g., $N_0\alpha = 0.19$ eV in the case of (Zn,Mn)Te [58]. An interesting situation occurs in III-V DMS with Mn^{3+} ions, in which ferromagnetic s - d coupling is compensated by antiferromagnetic exchange with holes tightly bound by Mn^{2+} ions [59], resulting in $N_0\alpha = 0.0 \pm 0.1$ eV in wz-(Ga,Mn)N [37].

Using notation and parameter values introduced in Secs. II, the p - d exchange energy for transition metal ions with the high-spin ($S = 2$) d^4 configuration is given by [30],

$$N_0\beta = V_{pd}^2 \left(\frac{1}{3} \frac{1}{E_d} + \frac{2}{15} \frac{1}{E_d + U} - \frac{7}{15} \frac{1}{E_d + U + J} \right), \quad (28)$$

where ($P_{\text{Te},p}$ projects the wavefunctions at Γ onto the p -symmetry orbitals of tellurium)

$$V_{pd} = \frac{4}{3} \left(V_{pd\sigma} - \frac{2}{\sqrt{3}} V_{pd\pi} \right) |\langle \psi_\Gamma | P_{\text{Te},p} | \psi_\Gamma \rangle|, \quad (29)$$

which results in

$$N_0\beta = -1.8 \pm 0.5 \text{ eV} \quad (30)$$

for $\text{Hg}_{1-x}\text{Cr}_x\text{Te}$ in the small x value limit and $E_d = -0.3 \pm 0.1$ eV, with an about 50% enhancement in the alternative model which includes the d - d hybridization. Large magnitudes of $N_0\alpha = 0.3$ and $N_0\beta = -1.8$ eV mean that full polarization of Cr spins in $\text{Hg}_{0.99}\text{Cr}_{0.01}\text{Te}$ will change E_g by about 21 meV, strongly affecting optical and transport properties.

In the same way, we can evaluate a magnitude of the upward shift ΔE_v of the $\text{Hg}_{1-x}\text{Cr}_x$ valence band top in

respect to HgTe, introduced by p - d hybridization,

$$\begin{aligned} \Delta E_v &= xN_0W_{pd} \\ &= -xV_{pd}^2 \left(\frac{1}{3} \frac{1}{E_d} + \frac{1}{5} \frac{1}{E_d + U} + \frac{7}{15} \frac{1}{E_d + U + J} \right) \end{aligned} \quad (31)$$

This equation leads to

$$N_0W_{pd} = 1.2 \pm 0.5 \text{ eV}, \quad (32)$$

for $\text{Hg}_{1-x}\text{Cr}_x\text{Te}$ in the small x limit. This value of N_0W_{pd} implies that p - d hybridization give a sizable contribution to the gap change. In particular, this fact is expected to enlarge the topological region, $E_g < 0$, to $x \approx 10\%$ in $\text{Hg}_{1-x}\text{Cr}_x\text{Te}$ compare to $\text{Hg}_{1-x}\text{Mn}_x\text{Te}$, where it extends to $x = 7\%$.

Particularly interesting is the case of $\text{Hg}_{1-x}\text{Cr}_x\text{Te}$ topological QWs. We assume that our evaluations of α and β magnitudes are correct and list out expected phenomena brought about by cation-substitutional randomly distributed Cr ions. In the paramagnetic phase, guided by the Mn case [60], we expect that the range of QW thicknesses corresponding to the topological phase shrinks with x , and the trivial phase occurs at any thicknesses for $x \gtrsim 0.07$ [61]. In the topological phase, two new effects of paramagnetic impurities upon the quantum spin Hall effect have been recently identified [62, 63]:

1. The formation of bound magnetic polarons by holes residing on residual acceptor impurities. The associated spin-splitting Δ of acceptor states diminishes spin-flip Kondo backscattering of edge electrons by acceptor holes at low temperatures, $k_B T \lesssim \Delta(T)$, where $\Delta(T)$ scales with $\chi(T)\mathcal{J}_{sp-d}^2$, where $\chi(T)$ is magnetic susceptibility of localized spins and \mathcal{J}_{sp-d}^2 is a weighted combination of α and β [63]. This model is experimentally corroborated by a recovery of the conductance quantization at low temperatures in topological $\text{Hg}_{1-x}\text{Mn}_x\text{Te}$ QWs [64].
2. Precessional dephasing of edge electron spins and momenta by a dense cloud of randomly oriented magnetic impurity spins. It has been argued that the constraint imposed by spin-momentum locking on the efficiency of backscattering by localized spins [65] is relaxed by a flow of spin momenta to the bath of interacting magnetic impurities [63]. This effect is relatively weakly dependent on temperature, as it scales with $T\chi(T)\mathcal{J}_{sp-d}^{\prime 2}$, where $\mathcal{J}_{sp-d}^{\prime 2}$ is another combination of α and β [63].

Interestingly, due to larger magnitudes of β and χ (enhanced by ferromagnetic components in J_{ij}), both effects are expected to be substantially stronger in $\text{Hg}_{1-x}\text{Cr}_x\text{Te}$ compared to $\text{Hg}_{1-x}\text{Mn}_x\text{Te}$.

Can one observe the anomalous quantum Hall effect in $\text{Hg}_{1-x}\text{Cr}_x\text{Te}$ quantum wells (QWs)? As we noted, there is a competition of FM and AFM interactions, so that either FM or spin-glass phase is expected at low temperatures. Furthermore, it was demonstrated that the

formation of a single chiral edge channels occurs for spin polarized magnetic ions along the growth direction, if $p = -\alpha/\beta \gtrsim 0.25$ [66], whereas the values quoted above point to $p = 0.17 \pm 0.1$. These two facts call for experimental verification. In the case of $p < 0.25$, polarization of Cr spins, either spontaneous or driven by an external magnetic field along the growth direction, will lead to the closure of the topological gap and the associated colossal drop of resistance.

We note, however, that the spin splitting of subbands with a heavy-hole character vanishes for the in-plane magnetization direction due to a competition between spin-orbit and p - d interactions [67]. This means that one can change the parameter p by tilting the magnetization direction. In order to verify this expectation we have adapted the eight bands' $k \cdot p$ model for the $\text{Hg}_{1-x}\text{Cr}_x\text{Te}$ quantum well surrounded by 30 nm-thick $\text{Hg}_{1-y}\text{Cd}_y\text{Te}$ barriers [63, 68]. We abandon the axial approximation and employ the values of $N_0\alpha$, $N_0\beta$, and N_0W_{pd} quoted above. The electron envelope function in the growth direction is taken as a linear combination of 51 Fourier components [69], whose contributions are obtained by diagonalization of the resulting 408×408 Hamiltonian \mathcal{H}_{k_x, k_y} assuming periodic boundary conditions in the z -direction [63].

Figure 10 shows the subband structure for unstrained 6 nm-thick $\text{Hg}_{0.97}\text{Cr}_{0.03}\text{Te}/\text{Hg}_{0.3}\text{Cd}_{0.7}\text{Te}$ QW in the absence of an external magnetic field. In the case of ferromagnetic (Hg,Cr)Te in a zinc-blende structure, for which cubic magnetic anisotropy is expected, the magnetization easy axis will assume either the $\langle 100 \rangle$ or $\langle 111 \rangle$ crystallographic direction. As seen in Fig. 10, for the easy axis along the growth direction, $\mathbf{M} \parallel [001]$, the presence of non-zero magnetization tends to close the gap, in agreement with the value $p < 0.25$. In contrast, for $\mathbf{M} \parallel [111]$, the topological gap persists and, moreover, the inverted band structure is present for the spin-down channel only. We conclude that the quantum anomalous Hall effect is expected under these conditions.

To substantiate the above conclusion, we have calculated Berry's curvature $\Omega^{(x,y)}(\mathbf{k})$ for the 306 occupied valence subbands, i.e., for the Fermi level in the gap. Its integral over the 2D Brillouin zone provides $2\pi\mathcal{C}$, where the Chern number \mathcal{C} is directly related to Hall conductivity, $\sigma_{xy} = (e^2/h)\mathcal{C}$. For the fcc lattice and (001) orientation of the QW, the 2D Brillouin zone is a square spanned on the $[11]$ and $[\bar{1}\bar{1}]$ of the length $G = 2\sqrt{2}\pi/a_0$, where a_0 is the lattice constant. The computation involves two steps. First, to ensure the periodicity of \mathcal{H}_k , we introduce a \mathbf{k} vector regularization, according to

$$k_i \rightarrow (G/2\pi) \sin(2\pi k_i/G) \quad (33)$$

$$k_i k_j \rightarrow (G/\pi)^2 \sin(\pi k_i/G) \sin(\pi k_j/G), \quad (34)$$

where the components k_1 and k_2 of the vectors in the Brillouin zone are related to k_x and k_y and their combi-

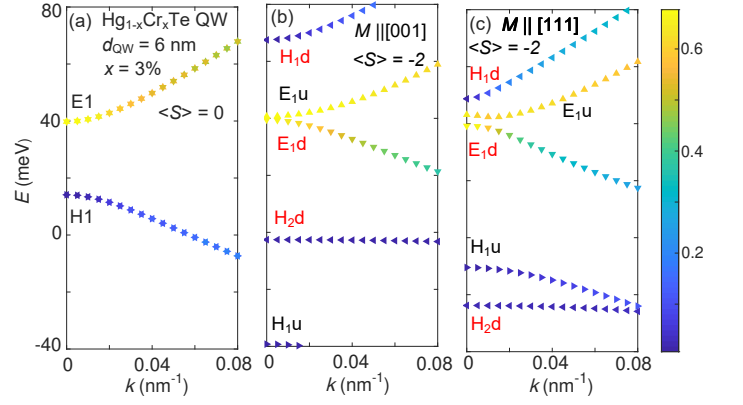


FIG. 10. Computed subband structure in unstrained $\text{Hg}_{0.97}\text{Cr}_{0.03}\text{Te}/\text{Hg}_{0.3}\text{Cd}_{0.7}\text{Te}$ quantum wells; labels H and E refer to subbands originating from the heavy-hole and electron-like bands in non-topological semiconductors; up and right oriented triangles correspond to spin-up orientation for subbands with the electron and hole character, respectively. (a) Paramagnetic case, i.e., average Cr spin $\langle S \rangle = 0$; (b) $\langle S \rangle = 2$ and magnetization is oriented along the growth direction; (c) $\langle S \rangle = 2$ and magnetization is oriented along the $[111]$ directions. Colors describe the participation of the $s_{1/2, \pm 1/2}$ Kohn-Luttinger amplitude in the electronic wave function; $\text{Hg}_{0.97}\text{Cr}_{0.03}\text{Te}$ QW thickness $d_{\text{QW}} = 6$ nm.

nations in the kp Hamiltonian by,

$$k_{x,y} = (k_1 \mp k_2)/\sqrt{2} \quad (35)$$

$$k_{x,y}^2 = (k_1 \mp k_2)^2/2 \quad (36)$$

$$k_x k_y = (k_1^2 - k_2^2)/2. \quad (37)$$

Second, we use the packet method introduced by Fukui *et al.* [70] in a numerically efficient implementation elaborated by Brzezicki [71], to calculate the total (a trace) of the Berry curvature over the occupied bands $E_n(\mathbf{k})$, $E_n(\mathbf{k}) < E_F$, as [72]

$$(\Delta k)^2 \Omega^{(x,y)}(\mathbf{k}) = \text{Im} \left\{ \text{Tr} \left[\prod_{i=1}^4 V_i V_i^\dagger \right] \right\}, \quad (38)$$

where Δk is the length of the packet side; V_i are matrices of eigenvectors whose columns correspond to the 306 eigenenergies $E_n(k_{i,1}, k_{i,2}) < E_F$ at the four wave vectors determining the packet position, $[k_1, k_2]$, $[k_1 + \Delta k, k_2]$, $[k_1 + \Delta k, k_2 + \Delta k]$, $[k_1, k_2 + \Delta k]$.

As shown in Fig. 11, non-zero Berry curvature weights for spin-polarized Cr ions, $S_{\text{av}} = -2$, reside in the Brillouin zone center, i.e., in the gap region. By computing $\Omega^{(x,y)}(\mathbf{k})(\Delta k)^2/2\pi$ values with adaptive Δk magnitudes over the whole 2D Brillouin zone, we obtained the Chern number $\mathcal{C} = 1.0$. We also checked that $\mathcal{C} = 0.00$ if $S_{\text{av}} = -0.1$, at which the band structure is no longer inverted. These outcomes confirm the prediction of the quantized Hall resistance.

Finally, we mention that in the case of (Zn,Cr)Te and (Ga,Mn)N the relevant donor level introduced by TM

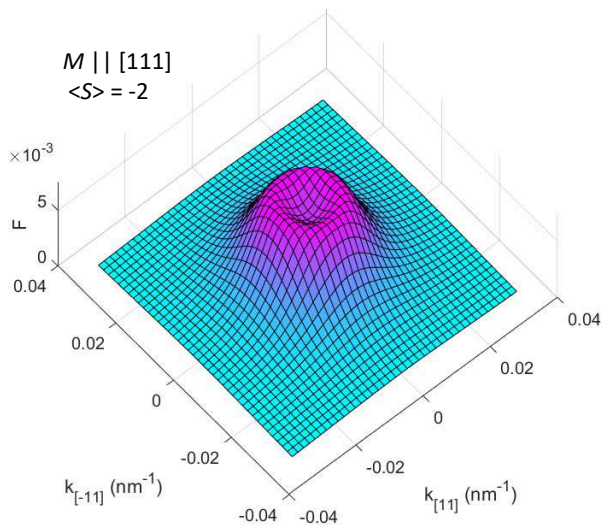


FIG. 11. Berry curvature integrated over the placket area $(\Delta k)^2$, $F(\mathbf{k})$, computed for the valence band subbands in a magnetized $\text{Hg}_{0.97}\text{Cr}_{0.03}\text{Te}/\text{Hg}_{0.3}\text{Cd}_{0.7}\text{Te}$ (001) QW quantum well, whose electronic structure is presented in Fig. 10(c). The data are shown for the Brillouin zone center (a side of the square is $G/400$), that provides the dominant contribution. The Chern number $C = 1.0$, obtained by summing up F values over the whole 2D Brillouin zone, indicates the presence of the quantum anomalous Hall effect.

ions resides in the gap, i.e., $E_d > 0$. In qualitative agreement with Eq. 28, the FM sign of β was observed in these two systems [37, 73]. However, as mentioned when discussing $N_0\alpha$ case, the Mn^3 state can be regarded as the Mn^{2+} acceptor with a tightly bound hole. The resulting bare coupling between a band hole and Mn^{2+} ion is then AFM. However, the experimentally proven existence of the hole bound state in the gap ($\text{Mn}^{3+/4+}$ complex with $E_d = 1.1\text{ eV}$) means that band hole can be trapped by Mn, meaning that the molecular-field approximation does not hold. A non-perturbative approach demonstrates that the apparent p - d coupling is FM under these conditions [35], in agreement with experimental findings [37].

VII. CONCLUSIONS AND OUTLOOK

We have presented the theoretical results for d - d and p - d exchange interactions in diluted magnetic insulators for the $S = 2$ case, i.e., for Cr in HgTe and ZnTe as well as for Mn in zinc-blende and wurtzite GaN. Our approach not only addresses some weak points of earlier theories of ferromagnetic superexchange but takes into account the interband Bloembergen-Rowland-Van Vleck and two-electron contributions. These additional terms

are of a lesser importance in (Ga,Mn)N but play a significant role in (Zn,Cr)Te and, particularly, in topological (Hg,Cr)Te, where they introduce antiferromagnetic coupling for certain pairs of Cr atoms. We have found that the presence of the competing interactions makes that the theoretical results become rather sensitive to the adopted tight-binding model of the host band structure. Because of this competition, and in agreement with experimental data, Curie temperatures T_C in (Zn,Cr)Te are expected to be lower compared to (Ga,Mn)N with the identical concentration of magnetic ions. At the same time, we cannot exclude the presence of a spin-glass phase rather than ferromagnetism in topological (Hg,Cr)Te. If this would be the case, a relatively large magnitude of the p - d exchange integral β that we predict for (Hg,Cr)Te should stabilize the quantum spin Hall effect by the formation of bound magnetic polarons that weaken Kondo backscattering of edge electrons by holes trapped to residual acceptor impurities. The large magnitude of β means also that the quantum anomalous Hall effect can be observed in topological (Hg,Cr)Te for the magnetization vector tilted away from the direction perpendicular to the quantum well plane, as confirmed by the Chern number determination.

Compared to ferromagnetic Bi-Sb chalcogenides, it is harder to introduce Cr and V to HgTe and related systems. However, once obtained, they should show lower areal density of native defects, as according to gating characteristics, the concentration of the in-gap localized states is almost two orders of magnitude smaller in HgTe quantum wells [74, 75] than in $(\text{Bi,Sb,Cr,V})_2\text{Te}_3$ layers [13, 14, 76]. As the exchange gap is typically in the dozen meV range (see Fig. 10), we assign the thermally activated conductivity σ_{xx} in $(\text{Bi,Sb,Cr,V})_2\text{Te}_3$ layers [13, 14, 76] to the Efros-Shklovskii hopping between in-gap states. A lower concentration of such states will allow for the operation of resistance standards at higher temperature.

ACKNOWLEDGMENTS

We acknowledge J. A. Majewski for sharing with us a code implementing formulas for superexchange (in the d^5 and d^4 cases) and W. Brzezicki for the Chern number formula. This research was supported by the Foundation for Polish Science through the IRA Programme cofinanced by EU within SG OP and EFSE (project ‘‘Mag-Top’’ no. FENG.02.01-IP.05-0028/23), by funds from the state budget allocated by the Minister of Science (Poland) as part of the Polish Metrology II programme project no. PM-II/SP/0012/2024/02, and by Interdisciplinary Centre for Mathematical and Computational Modelling, University of Warsaw (ICM UW) under computational allocations numbers G93-1595 and G93-1601.

Appendix A: Transformation matrix to $T_2 \oplus E$

With the threefold wurtzite c -axis as the z (quantization) axis, a symmetry-invariant decomposition of the Hilbert space for $L = 2$ into $3 + 2$ dimensions ($T_2 \oplus E$) is parameterized below by (θ, ϕ) [cf. Eq. 68 of Ref. 19]. The threefold symmetry acts by cycling the T_2 vectors $(\psi_{T_2,i})_{i=1,2,3}$. Under cubic symmetry, $\cos(\theta) = 1/\sqrt{3}$; the deviation from this value is a material parameter. On the other hand, due to the wurtzite mirror symmetry, ϕ is not variable, but it takes different and conventions-dependent values for the two inequivalent cation positions [77] (here, $\phi = -\pi/2$ for t_2 and $\phi = \pi/2$ for t_4).

$$\langle yz | \psi_{T_2,1} \rangle = \sqrt{2/3} \cos(\theta) \sin(\phi) \quad (\text{A1})$$

$$\langle xz | \psi_{T_2,1} \rangle = -\sqrt{2/3} \cos(\theta) \cos(\phi) \quad (\text{A2})$$

$$\langle xy | \psi_{T_2,1} \rangle = -\sqrt{2/3} \sin(\theta) \sin(2\phi) \quad (\text{A3})$$

$$\langle 3z^2 - r^2 | \psi_{T_2,1} \rangle = \sqrt{1/3} \quad (\text{A4})$$

$$\langle x^2 - y^2 | \psi_{T_2,1} \rangle = \sqrt{2/3} \sin(\theta) \cos(2\phi) \quad (\text{A5})$$

$$\langle yz | \psi_{T_2,2} \rangle = -\cos \theta \left[3 \cos(\phi) + \sqrt{3} \sin(\phi) \right] / (3\sqrt{2}) \quad (\text{A6})$$

$$\langle xz | \psi_{T_2,2} \rangle = \cos \theta \left[\cos(\phi) / \sqrt{6} - \sin(\phi) / \sqrt{2} \right] \quad (\text{A7})$$

$$\langle xy | \psi_{T_2,2} \rangle = -\sin \theta \left[\cos(2\phi) / \sqrt{2} - \sin(2\phi) / \sqrt{6} \right] \quad (\text{A8})$$

$$\langle 3z^2 - r^2 | \psi_{T_2,2} \rangle = \sqrt{1/3} \quad (\text{A9})$$

$$\langle x^2 - y^2 | \psi_{T_2,2} \rangle = -\sin \theta \left[\sqrt{3} \cos(2\phi) + 3 \sin(2\phi) \right] / (3\sqrt{2}) \quad (\text{A10})$$

$$\langle yz | \psi_{T_2,3} \rangle = \cos \theta \left[\cos(\phi) / \sqrt{2} - \sin(\phi) / \sqrt{6} \right] \quad (\text{A11})$$

$$\langle xz | \psi_{T_2,3} \rangle = \cos \theta \left[\cos(\phi) / \sqrt{6} + \sin(\phi) / \sqrt{2} \right] \quad (\text{A12})$$

$$\langle xy | \psi_{T_2,3} \rangle = \sin \theta \left[\cos(2\phi) / \sqrt{2} + \sin(2\phi) / \sqrt{6} \right] \quad (\text{A13})$$

$$\langle 3z^2 - r^2 | \psi_{T_2,3} \rangle = \sqrt{1/3} \quad (\text{A14})$$

$$\langle x^2 - y^2 | \psi_{T_2,3} \rangle = -\sin \theta \left[\cos(2\phi) / \sqrt{6} - \sin(2\phi) / \sqrt{2} \right] \quad (\text{A15})$$

$$\langle yz | \psi_{E,1} \rangle = -\sin \theta [\cos(\phi) + \sin(\phi)] / \sqrt{2} \quad (\text{A16})$$

$$\langle xz | \psi_{E,1} \rangle = \sin \theta \left[\cos(\phi) / \sqrt{6} + \sin(\phi) / \sqrt{2} \right] \quad (\text{A17})$$

$$\langle xy | \psi_{E,1} \rangle = \cos \theta [\cos(\phi) - \sin(\phi)] / \sqrt{2} \quad (\text{A18})$$

$$\langle 3z^2 - r^2 | \psi_{E,1} \rangle = 0 \quad (\text{A19})$$

$$\langle x^2 - y^2 | \psi_{E,1} \rangle = \cos \theta [\cos(2\phi) + \sin(2\phi)] / \sqrt{2} \quad (\text{A20})$$

$$\langle yz | \psi_{E,2} \rangle = \sin \theta [\cos(\phi) - \sin(\phi)] / \sqrt{2} \quad (\text{A21})$$

$$\langle xz | \psi_{E,2} \rangle = \sin \theta [\cos(\phi) + \sin(\phi)] / \sqrt{2} \quad (\text{A22})$$

$$\langle xy | \psi_{E,2} \rangle = -\cos \theta [\cos(2\phi) + \sin(2\phi)] / \sqrt{2} \quad (\text{A23})$$

$$\langle 3z^2 - r^2 | \psi_{E,2} \rangle = 0 \quad (\text{A24})$$

$$\langle x^2 - y^2 | \psi_{E,2} \rangle = \cos \theta [\cos(2\phi) - \sin(2\phi)] / \sqrt{2} \quad (\text{A25})$$

Appendix B: Definitions of the correlation lengths

($\mathbf{r} = x_1 \mathbf{a}_1 + x_2 \mathbf{a}_2 + x_3 \mathbf{a}_3$) as:

The definition of the correlation length varies from a crystal structure to another. For wurtzite, we assume that the correlator decays exponentially with distance

$$C(\mathbf{r}) = \exp\left(-\frac{(|x_1| + |x_2| + |x_1 + x_2|)}{\xi_a}\right) \exp\left(-\frac{|x_3|}{\xi_c}\right). \quad (\text{B1})$$

We estimate ξ_c as follows: a simulation is performed in a lattice block of size $L_1 \times L_2 \times L_3$, $L_1/L_3 = L_2/L_3 = 3/2$, and the susceptibility $\chi_{k=k_{min,c}}$ at momentum $k_{min,c} = (k_1, k_2, k_3) = (0, 0, \frac{4\pi}{L_3})$, together with magnetization squared (i.e. the susceptibility at zero momentum, $k_1 = k_2 = k_3 = 0$), are both evaluated. We define $\xi_{wz,c} \approx \xi_c$ as

$$\xi_{wz,c} \approx \frac{1}{3 \sin \frac{4\pi}{3L_3}} \sqrt{\frac{\chi_{k=0}}{\chi_{k=k_{min,c}}} - 1}. \quad (B2)$$

Analogously, $\xi_{wz,a} \approx \xi_a$ can be defined as

$$\xi_{wz,a} \approx \frac{7}{18 \sin \frac{2\pi}{L_1}} \sqrt{\frac{\chi_{k=0}}{\chi_{k=k_{min,a}}} - 1}, \quad (B3)$$

$$\text{with } k_{min,a} = \left(\frac{6\pi}{L_1}, 0, 0\right).$$

-
- [1] T. Dietl and H. Ohno, “Dilute ferromagnetic semiconductors: Physics and spintronic structures,” *Rev. Mod. Phys.* **86**, 187–251 (2014).
- [2] T. Jungwirth, J. Wunderlich, V. Novák, K. Olejník, B. L. Gallagher, R. P. Campion, K. W. Edmonds, A. W. Rushforth, A. J. Ferguson, and P. Němec, “Spin-dependent phenomena and device concepts explored in (Ga,Mn)As,” *Rev. Mod. Phys.* **86**, 855–896 (2014).
- [3] D. Szentkiel, M. Foltyn, G. P. Mazur, R. Adhikari, K. Kosiel, K. Gas, M. Zgirski, R. Kruszka, R. Jakiela, Tian Li, A. Piotrowska, A. Bonanni, M. Sawicki, and T. Dietl, “Stretching magnetism with an electric field in a nitride semiconductor,” *Nat. Commun.* **7**, 13232 (2016).
- [4] M. Mogi, Y. Okamura, M. Kawamura, R. Yoshimi, K. Yasuda, A. Tsukazaki, K. S. Takahashi, T. Morimoto, N. Nagaosa, M. Kawasaki, Y. Takahashi, and Y. Tokura, “Experimental signature of the parity anomaly in a semi-magnetic topological insulator,” *Nat. Phys.* **18**, 390–394 (2022).
- [5] Rui Yu, Wei Zhang, Hai-Jun Zhang, Shou-Cheng Zhang, Xi Dai, and Zhong Fang, “Quantized anomalous Hall effect in magnetic topological insulators,” *Science* **329**, 61–64 (2010).
- [6] Cui-Zu Chang, Jinsong Zhang, Xiao Feng, Jie Shen, Zuo-cheng Zhang, Minghua Guo, Kang Li, Yunbo Ou, Pang Wei, Li-Li Wang, Zhong-Qing Ji, Yang Feng, Shuai-hua Ji, Xi Chen, Jinfeng Jia, Xi Dai, Zhong Fang, Shou-Cheng Zhang, Ke He, Yayu Wang, Li Lu, Xu-Cun Ma, and Qi-Kun Xue, “Experimental observation of the quantum anomalous Hall effect in a magnetic topological insulator,” *Science* **340**, 167–170 (2013).
- [7] He Ke, Yayu Wang, and Qi-Kun Xue, “Topological materials: quantum anomalous Hall system,” *Annu. Rev. Cond. Mat. Phys.* **9**, 329–344 (2018).
- [8] Y. Tokura, K. Yasuda, and A. Tsukazaki, “Magnetic topological insulators,” *Nat. Rev. Phys.* **1**, 126–143 (2019).
- [9] B. A. Bernevig, C. Felser, and H. Beidenkopf, “Progress and prospects in magnetic topological materials,” *Nature* **603**, 41–51 (2022).
- [10] Cui-Zu Chang, Chao-Xing Liu, and A. H. MacDonald, “Quantum anomalous Hall effect,” *Rev. Mod. Phys.* **95**, 011002 (2023).
- [11] M. Goetz, K. M. Fijalkowski, E. Pesel, M. Hartl, S. Schreyeck, M. Winnerlein, S. Grauer, H. Scherer, K. Brunner, C. Gould, F. J. Ahlers, and L. W. Molenkamp, “Precision measurement of the quantized anomalous Hall resistance at zero magnetic field,” *Appl. Phys. Lett.* **112**, 072102 (2018).
- [12] E. J. Fox, I. T. Rosen, Yanfei Yang, G. R. Jones, R. E. Elmquist, Xufeng Kou, Lei Pan, Kang L. Wang, and D. Goldhaber-Gordon, “Part-per-million quantization and current-induced breakdown of the quantum anomalous Hall effect,” *Phys. Rev. B* **98**, 075145 (2018).
- [13] Y. Okazaki, T. Oe, M. Kawamura, R. Yoshimi, S. Nakamura, S. Takada, M. Mogi, K. S. Takahashi, A. Tsukazaki, M. Kawasaki, Y. Tokura, and N.-H. Kaneko, “Quantum anomalous Hall effect with a permanent magnet defines a quantum resistance standard,” *Nat. Phys.* **18**, 25 (2022).
- [14] L. K. Rodenbach, Ngoc Thanh Mai Tran, J. M. Underwood, A. R. Panna, M. P. Andersen, Z. S. Barcikowski, S. U. Payagala, Peng Zhang, Lixuan Tai, Kang L. Wang, R. E. Elmquist, D. G. Jarrett, D. B. Newell, A. F. Rigosi, and D. Goldhaber-Gordon, “Realization of the quantum ampere using the quantum anomalous Hall and Josephson effects,” *arXiv:2308.00200* (2023), 10.48550/arXiv.2308.00200.
- [15] T. R. F. Peixoto, H. Bentmann, P. Rüßmann, A.-V. Tcakaev, M. Winnerlein, S. Schreyeck, S. Schatz, R. C. Vidal, F. Stier, V. Zabolotnyy, R. J. Green, Chul Hee Min, C. I. Fornari, Maaß H., H. B. Vasili, P. Gargiani, M. Valvidares, A. Barla, J. Buck, M. Hoesch, F. Diekmann, S. Rohlf, M. Kalläne, K. Rosnagel, Ch. Gould, K. Brunner, S. Blügel, V. Hinkov, L. W. Molenkamp, and F. Reinert, “Non-local effect of impurity states on the exchange coupling mechanism in magnetic topological insulators,” *npj Quant. Mater.* **5**, 87 (2020).
- [16] C. Śliwa, C. Autieri, J. A. Majewski, and T. Dietl, “Superexchange dominates in magnetic topological insulators,” *Phys. Rev. B* **104**, L220404 (2021).
- [17] R. Watanabe, R. Yoshimi, M. Kawamura, M. Mogi, A. Tsukazaki, X. Z. Yu, K. Nakajima, K. S. Takahashi, M. Kawasaki, and Y. Tokura, “Quantum anomalous Hall effect driven by magnetic proximity coupling in all-telluride based heterostructure,” *Appl. Phys. Lett.* **115**, 102403 (2019).
- [18] S. D. Escribano, A. Maiani, M. Leijnse, K. Flensberg, Y. Oreg, A. Levy Yeyati, E. Prada, and R. Seoane Souto, “Semiconductor-ferromagnet-superconductor planar heterostructures for 1D topological superconductivity,” *npj Quant. Mater.* **7**, 81 (2022).
- [19] John B. Goodenough, *Magnetism and the Chemical Bond*, Interscience Monographs on Chemistry (Interscience Publishers, 1963).
- [20] J. Blinowski, P. Kacman, and J. A. Majewski, “Ferromagnetic superexchange in Cr-based diluted magnetic semiconductors,” *Phys. Rev. B* **53**, 9524–9527 (1996).

- [21] S. Kuroda, N. Nishizawa, K. Takita, M. Mitome, Y. Bando, K. Osuch, and T. Dietl, “Origin and control of high-temperature ferromagnetism in semiconductors,” *Nat. Mater.* **6**, 440 (2007).
- [22] E. Sarigiannidou, F. Wilhelm, E. Monroy, R. M. Galera, E. Bellet-Amalric, A. Rogalev, J. Goulon, J. Cibert, and H. Mariette, “Intrinsic ferromagnetism in wurtzite (Ga,Mn)N semiconductor,” *Phys. Rev. B* **74**, 041306 (2006).
- [23] M. Sawicki, T. Devillers, S. Gałęski, C. Simserides, S. Dobkowska, B. Faina, A. Grois, A. Navarro-Quezada, K. N. Trohidou, J. A. Majewski, T. Dietl, and A. Bonanni, “Origin of low-temperature magnetic ordering in $\text{Ga}_{1-x}\text{Mn}_x\text{N}$,” *Phys. Rev. B* **85**, 205204 (2012).
- [24] S. Stefanowicz, G. Kunert, C. Simserides, J. A. Majewski, W. Stefanowicz, C. Kruse, S. Figge, Tian Li, R. Jakiela, K. N. Trohidou, A. Bonanni, D. Hommel, M. Sawicki, and T. Dietl, “Phase diagram and critical behavior of the random ferromagnet $\text{Ga}_{1-x}\text{Mn}_x\text{N}$,” *Phys. Rev. B* **88**, 081201(R) (2013).
- [25] C. Simserides, J.A. Majewski, K.N. Trohidou, and T. Dietl, “Theory of ferromagnetism driven by superexchange in dilute magnetic semiconductors,” *EPJ Web of Conferences* **75**, 01003 (2014).
- [26] N. Bloembergen and T. J. Rowland, “Nuclear spin exchange in solids: Tl^{203} and Tl^{205} magnetic resonance in thallium and thallic oxide,” *Phys. Rev.* **97**, 1679–1698 (1955).
- [27] C. Lewiner, J. Gaj, and G. Bastard, “Indirect exchange interaction in $\text{Hg}_{1-x}\text{Mn}_x\text{Te}$ and $\text{Cd}_{1-x}\text{Mn}_x\text{Te}$ alloys,” *J. Phys. Colloq. (Paris)* **41 (C5)**, 289–292 (1980).
- [28] B. E. Larson, K. C. Hass, H. Ehrenreich, and A. E. Carlsson, “Theory of exchange interactions and chemical trends in diluted magnetic semiconductors,” *Phys. Rev. B* **37**, 4137–4154 (1988).
- [29] T. Dietl, H. Ohno, and F. Matsukura, “Hole-mediated ferromagnetism in tetrahedrally coordinated semiconductors,” *Phys. Rev. B* **63**, 195205 (2001).
- [30] P. Kacman, “Spin interactions in diluted magnetic semiconductors and magnetic semiconductor structures,” *Semicon. Sci. Technol.* **16**, R25–R39 (2001).
- [31] C. Śliwa and T. Dietl, “Thermodynamic perturbation theory for noninteracting quantum particles with application to spin-spin interactions in solids,” *Phys. Rev. B* **98**, 035105 (2018).
- [32] I. Ya. Korenblit, E. F. Shender, and B. I. Shklovsky, “Percolation approach to the phase transition in very dilute ferromagnetic alloys,” *Phys. Lett. A* **46**, 275–276 (1973).
- [33] K. Sato, L. Bergqvist, J. Kudrnovský, P. H. Dederichs, O. Eriksson, I. Turek, B. Sanyal, G. Bouzerar, H. Katayama-Yoshida, V. A. Dinh, T. Fukushima, H. Kizaki, and R. Zeller, “First-principles theory of dilute magnetic semiconductors,” *Rev. Mod. Phys.* **82**, 1633–1690 (2010).
- [34] A. Bonanni, T. Dietl, and H. Ohno, “Dilute magnetic materials,” in *Handbook of Magnetism and Magnetic Materials*, edited by M. Coey and S. Parkin (Springer, Berlin, 2021).
- [35] T. Dietl, “Hole states in wide band-gap diluted magnetic semiconductors and oxides,” *Phys. Rev. B* **77**, 085208 (2008).
- [36] W. Mac, A. Twardowski, and M. Demianiuk, “s,p-d exchange interaction in Cr-based diluted magnetic semiconductors,” *Phys. Rev. B* **54**, 5528–5535 (1996).
- [37] J. Suffczyński, A. Grois, W. Pacuski, A. Golnik, J. A. Gaj, A. Navarro-Quezada, B. Faina, T. Devillers, and A. Bonanni, “Effects of *s,p-d* and *s-p* exchange interactions probed by exciton magnetospectroscopy in (Ga,Mn)N,” *Phys. Rev. B* **83**, 094421 (2011).
- [38] Chao-Xing Liu, Xiao-Liang Qi, Xi Dai, Zhong Fang, and Shou-Cheng Zhang, “Quantum Anomalous Hall Effect in $\text{Hg}_{1-y}\text{Mn}_y\text{Te}$ Quantum Wells,” *Phys. Rev. Lett.* **101**, 146802 (2008).
- [39] S. Kuroda, N. Nishizawa, K. Takita, M. Mitome, Y. Bando, K. Osuch, and T. Dietl, “Origin and control of high-temperature ferromagnetism in semiconductors,” *Nat. Mater.* **6**, 440–446 (2007).
- [40] Tobias Graf, Sebastian T. B. Goennenwein, and Martin S. Brandt, “Prospects for carrier-mediated ferromagnetism in GaN,” *physica status solidi (b)* **239**, 277–290 (2003).
- [41] B. Han, B. W. Wessels, and M. P. Ulmer, “Optical investigation of electronic states of Mn^{4+} ions in *p*-type GaN,” *Appl. Phys. Lett.* **86**, 042505 (2005).
- [42] J. I. Hwang, Y. Ishida, M. Kobayashi, H. Hirata, K. Takubo, T. Mizokawa, A. Fujimori, J. Okamoto, K. Mamiya, Y. Saito, Y. Muramatsu, H. Ott, A. Tanaka, T. Kondo, and H. Munekata, “High-energy spectroscopic study of the III–V nitride-based diluted magnetic semiconductor $\text{Ga}_{1-x}\text{Mn}_x\text{N}$,” *Phys. Rev. B* **72**, 085216 (2005).
- [43] D. Bertho, D. Boiron, A. Simon, C. Jouanin, and C. Priester, “Calculation of hydrostatic and uniaxial deformation potentials with a self-consistent tight-binding model for Zn-cation-based II–VI compounds,” *Phys. Rev. B* **44**, 6118–6124 (1991).
- [44] Lei Shi and Dimitrios A. Papaconstantopoulos, “Modifications and extensions to Harrison’s tight-binding theory,” *Phys. Rev. B* **70**, 205101 (2004).
- [45] R. H. Parmenter, “Effect of orbital degeneracy on the Anderson model of a localized moment in a metal,” *Phys. Rev. B* **8**, 1273–1275 (1973).
- [46] Roland Winkler, *Spin-orbit coupling effects in two-dimensional electron systems* (Springer Verlag, Berlin, Heidelberg, 2003).
- [47] A. I. Liechtenstein, M. I. Katsnelson, and V. A. Gubanov, “Exchange interactions and spin-wave stiffness in ferromagnetic metals,” *J. Phys. F: Met. Phys.* **14**, L125 (1984).
- [48] Guy Allan and Christophe Delerue, “Tight-binding calculations of the optical properties of HgTe nanocrystals,” *Phys. Rev. B* **86**, 165437 (2012).
- [49] Sameer Sapra, N. Shanthi, and D. D. Sarma, “Realistic tight-binding model for the electronic structure of II–VI semiconductors,” *Phys. Rev. B* **66**, 205202 (2002).
- [50] J. Spalek, A. Lewicki, Z. Tarnawski, J. K. Furdyna, R. R. Galazka, and Z. Obuszko, “Magnetic susceptibility of semimagnetic semiconductors: The high-temperature regime and the role of superexchange,” *Phys. Rev. B* **33**, 3407–3418 (1986).
- [51] A. Bonanni, M. Sawicki, T. Devillers, W. Stefanowicz, B. Faina, Tian Li, T. E. Winkler, D. Sztienkiel, A. Navarro-Quezada, M. Rovezzi, R. Jakiela, A. Grois, M. Wegscheider, W. Jantsch, J. Suffczyński, F. D’Acapito, A. Meingast, G. Kothleitner, and T. Dietl, “Experimental probing of exchange interactions between localized spins in the dilute magnetic insulator (Ga,Mn)N,” *Phys. Rev. B* **84**, 035206 (2011).

- [52] Giuseppe Cuono, Carmine Autieri, and Tomasz Dietl, “CdTe and HgTe doped with V, Cr, and Mn — prospects for the quantum anomalous Hall effect,” (2023), arXiv:2312.16732 [cond-mat.mtrl-sci].
- [53] C. Śliwa, “Disorder-averaged Binder ratio in site-diluted Heisenberg $\text{Hg}_{1-x}\text{Mn}_x\text{Te}$,” (2022), arXiv:2205.00977.
- [54] L. Brey and G. Gómez-Santos, “Magnetic properties of $(\text{Ga},\text{Mn})\text{As}$ from an effective Heisenberg Hamiltonian,” *Phys. Rev. B* **68**, 115206 (2003).
- [55] M. Dobrowolska and W. Dobrowolski, “Temperature study of interband magnetoabsorption in $\text{Hg}_{1-x}\text{Mn}_x\text{Te}$ mixed crystals,” *J. Phys. C: Solid State Phys.* **14**, 5689 (1981).
- [56] G. Bauer, J. Kossut, R. Faymonville, and R. Dornhaus, “Magnetorefectivity study of the band structure of $\text{Hg}_{1-x}\text{Mn}_x\text{Te}$ ($0.026 \leq x \leq 0.106$),” *Phys. Rev. B* **31**, 2040–2048 (1985).
- [57] C. Autieri, C. Śliwa, R. Islam, G. Cuono, and T. Dietl, “Momentum-resolved spin splitting in Mn-doped trivial CdTe and topological HgTe semiconductors,” *Phys. Rev. B* **103**, 115209 (2021).
- [58] A. Twardowski, P. Swiderski, M. von Ortenberg, and R. Pauthenet, “Magnetoabsorption and magnetization of $\text{Zn}_{1-x}\text{Mn}_x\text{Te}$ mixed crystals,” *Solid State Commun.* **50**, 509–513 (1984).
- [59] Cezary Śliwa and Tomasz Dietl, “Electron-hole contribution to the apparent $s - d$ exchange interaction in III-V dilute magnetic semiconductors,” *Phys. Rev. B* **78**, 165205 (2008).
- [60] S. Shamim, W. Beugeling, J. Böttcher, P. Shekhar, A. Budewitz, P. Leubner, L. Lunczer, E. M. Hankiewicz, H. Buhmann, and L. W. Molenkamp, “Emergent quantum Hall effects below 50 mT in a two-dimensional topological insulator,” *Adv. Sci.* **6**, eaba4625 (2020).
- [61] M. Sawicki, T. Dietl, W. Plesiewicz, P. Sękowski, L. Śniadower, M. Baj, and L. Dmowski, “Influence of an acceptor state on transport in zero-gap $\text{Hg}_{1-x}\text{Mn}_x\text{Te}$,” in *Application of High Magnetic Fields in Semiconductor Physics*, edited by G. Landwehr (Springer Berlin Heidelberg, Berlin, Heidelberg, 1983) pp. 382–385.
- [62] T. Dietl, “Effects of charge dopants in quantum spin Hall materials,” *Phys. Rev. Lett.* **130**, 086202 (2023).
- [63] T. Dietl, “Quantitative theory of backscattering in topological HgTe and $(\text{Hg},\text{Mn})\text{Te}$ quantum wells: Acceptor states, Kondo effect, precessional dephasing, and bound magnetic polaron,” *Phys. Rev. B* **107**, 085421 (2023).
- [64] S. Shamim, W. Beugeling, P. Shekhar, K. Bendias, L. Lunczer, J. Kleinlein, H. Buhmann, and L. W. Molenkamp, “Quantized spin Hall conductance in a magnetically doped two dimensional topological insulator,” *Nat. Commun.* **12**, 3193 (2021).
- [65] Y. Tanaka, A. Furusaki, and K. A. Matveev, “Conductance of a helical edge liquid coupled to a magnetic impurity,” *Phys. Rev. Lett.* **106**, 236402 (2011).
- [66] Chao-Xing Liu, Xiao-Liang Qi, Xi Dai, Zhong Fang, and Shou-Cheng Zhang, “Quantum anomalous Hall effect in $\text{Hg}_{1-y}\text{Mn}_y\text{Te}$ quantum wells,” *Phys. Rev. Lett.* **101**, 146802 (2008).
- [67] T. F. Ren, A. Wasiela, Y. Merle d’Aubigné, D. E. Ashenford, and B. Lunn, “Anisotropy of the zeeman effect in $\text{CdTe}/\text{Cd}_{1-x}\text{Mn}_x\text{Te}$ multiple quantum wells,” *Phys. Rev. B* **47**, 3783–3789 (1993).
- [68] E. G. Novik, A. Pfeuffer-Jeschke, T. Jungwirth, V. Latussek, C. R. Becker, G. Landwehr, H. Buhmann, and L. W. Molenkamp, “Band structure of semimagnetic $\text{Hg}_{1-y}\text{Mn}_y\text{Te}$ quantum wells,” *Phys. Rev. B* **72**, 035321 (2005).
- [69] Boundary terms at the well-barrier interfaces are neglected.
- [70] Takahiro Fukui, Yasuhiro Hatsugai, and Hiroshi Suzuki, “Chern numbers in discretized Brillouin zone: Efficient method of computing (spin) Hall conductances,” *J. Phys. Soc. Jpn.* **74**, 1674–1677 (2005).
- [71] W. Brzezicki, Unpublished.
- [72] If the presence of degenerate bands cannot be excluded, the determinants of the submatrices corresponding to each of the mutually different eigenenergies must be computed instead. Then the imaginary part of the trace can be obtained as the logarithm of the product of all the determinants (normalized to the unit circle), and is the Abelian curvature of the adiabatic transport of full-dimension orthonormal sets of energy eigenstates. Considering the principal branch of the logarithm [70] eliminates ambiguity of the result.
- [73] A. Twardowski, H. J. M. Swagten, W. J. M. de Jonge, and M. Demianiuk, “Magnetic behavior of the diluted magnetic semiconductor $\text{Zn}_{1-x}\text{Mn}_x\text{Se}$,” *Phys. Rev. B* **36**, 7013–7023 (1987).
- [74] K. Bendias, S. Shamim, O. Herrmann, A. Budewitz, P. Shekhar, P. Leubner, J. Kleinlein, E. Bocquillon, H. Buhmann, and L. W. Molenkamp, “High mobility HgTe microstructures for quantum spin Hall studies,” *Nano Lett.* **18**, 4831–4836 (2018).
- [75] I. Yahniiuk, A. Kazakov, B. Jouault, S. S. Krishtopenko, S. Kret, G. Grabecki, G. Cywiński, N. N. Mikhailov, S. A. Dvoretzkii, J. Przybytek, V. I. Gavrilenco, F. Teppe, T. Dietl, and W. Knap, “HgTe quantum wells for QHE metrology under soft cryomagnetic conditions: permanent magnets and liquid ^4He temperatures,” 10.48550/arXiv.2111.07581.
- [76] K. M. Fijalkowski, Nan Liu, P. Mandal, S. Schreyeck, K. Brunner, C. Gould, and L. W. Molenkamp, “Quantum anomalous Hall edge channels survive up to the Curie temperature,” *Nat. Commun.* **12**, 5599 (2021).
- [77] Tao Yang, Sadanojo Nakajima, and Shiro Sakai, “Electronic structures of wurtzite GaN, InN and their alloy $\text{Ga}_{1-x}\text{In}_x\text{N}$ calculated by the tight-binding method,” *Jpn. J. Appl. Phys.* **34**, 5912 (1995).